Summer 2024

Microwave Materials Characterization of Geopolymers

Jared Sinkey
Missouri University of Science and Technology

Department:

MIRCROWAVE MATERIALS CHARACTERIZATION OF GEOPOLYMERS

by

JARED DANIEL SINKEY

A THESIS

Presented to the Graduate Faculty of the

MISSOURI UNIVERSITY OF SCIENCE AND TECHNOLOGY

In Partial Fulfillment of the Requirements for the Degree

MASTER OF SCIENCE IN ELECTRICAL ENGINEERING

2024

Approved by:

Kristen Donnell, Advisor
DongHyun Kim
Chulsoon Hwang

ABSTRACT

The purpose of this work was to develop a process for studying geopolymer materials using a microwave materials characterization approach. Such an approach is known to provide information about chemical and physical properties of materials. As such, in this work, the focus is on the role of water in the geopolymer curing process. To do this, specimens were prepared and cast and microwave measurements conducted throughout the curing process using a short-circuited rectangular waveguide (SC-RWG) measurement technique. In this technique, the complex reflection properties/coefficient of the sample are measured. The effect of sample length and dielectric properties on materials characterization measurements using the short-circuited rectangular waveguide approach was studied and determined that samples placed at the shorted end can be reliably measured (contrary to the existing literature). Concurrent to the measurement effort, a dielectric mixing model was applied to relate the volumetric content and dielectric properties of the geopolymer constituents to the overall dielectric properties of the cast and cured geopolymer. The calculated dielectric properties (from the mixing model) were used as an input to a full wave simulation model. This simulation model provides the reflection properties of a material within a SC-RWG sample holder. The simulated results were compared to the geopolymer's measured reflection properties. Though these simulations did not agree well with measurements, a reliable process was created to be used on further geopolymer measurements. In addition, conclusions were made regarding how to improve the overall approach for future materials.

ACKNOWLEDGMENTS

I would like to extend my most sincere gratitude to Dr. Donnell, my advisor, for continued support over my graduate career, and investing abundant time and effort into my education and career. I am so grateful to my colleagues at the *u*Sense lab for all of your help, whether it be taking measurements at odd hours, providing your insights, or being great classmates. I would like to thank my committee members, Dr. Kim and Dr. Hwang, for their roles not only as members of my committee, but also as great instructors. Thank you to Dr. Shearer and the South Dakota School of Mines and Technology for providing samples, materials, information, and wisdom that made this work possible. This study was partially funded by the National Science Foundation.

Thank you to my parents for always believing in me, and your encouragement through challenges and triumphs alike. I am so thankful for the long-lasting friends I have made throughout my time at S&T. I am so honored to have had the best roommates and floormates, and your friendships have been the highlight of my collegiate experience. Sydney, thank you for your love, inspiring creativity, and reassurance. Without you, this work would have been impossible.

TABLE OF CONTENTS

LIST OF ILLUSTRATIONS

Page

LIST OF TABLES

Page

NOMENCLATURE

Symbol	Description
ε_r	Complex Relative Permittivity
λ	Wavlength

1. INTRODUCTION

1.1. BACKGROUND AND MOTIVATION – GEOPOLYMER MATERIALS

Geopolymers are an alkali activated material that are viewed as a potential alternative to Ordinary Portland Cement (OPC) concrete [1],[2]. They are able to provide tensile and flexural strength similar to that of OPC concrete, but impose a lighter carbon footprint, since there is no high temperature calcination during the reaction [2]. Geopolymer precursor powders, a key component used to create them, are often by-products from industrial applications, which adds to the sustainability of geopolymers [1]. Geopolymers are formed by mixing an alkali solution, such as Sodium Hydroxide or Alumino Silicate, with a precursor powder, such as fly ash or metakaolin [3]. These materials can potentially be used in many civil and architectural applications, and geopolymer concrete is already in use in some commercial and residential buildings. However, before such implementation can be done on a large-scale level in society, a more detailed understanding as to the curing process and the chemical reactions that take place is needed. This includes the role of water during the reaction. More specifically, the binding state of water changes during the reaction, as the water changes state from free to bound and vice versa (depending on the specific mix design) during the reaction. Microwave measurements in R-band (1.7-2.6 GHz) and S-band (2.6-3.95 GHz) have been sown to be particularly sensitive to bound and free water, respectively [4]. As such, these frequency bands will be used in this work to attempt to better understand the binding state of water in geopolymer reactions. To this end, this work proposes a microwave materials characterization approach to study the role of water in the

geopolymer curing reaction. Specifically, a set of geopolymer samples were cast with different alkaline solutions that were subsequently cured at different temperatures, with microwave measurements conducted throughout the curing cycle in order achieve this goal.

1.2. MICROWAVE MATERIALS CHARACTERIZATION

Microwave materials characterization is an important aspect of microwave NDT&E (Nondestructive Testing and Evaluation), where microwave (reflection and/or transmission) measurements are made on a material of interest [5],[6]. These measurements are used to calculate the dielectric properties of the material, which can subsequently be related to important chemical and physical properties [4],[7],[8]. Dielectric properties are intrinsic, which means they are independent of the measurement technique. Often referenced to free space, dielectric properties are defined as $\varepsilon_r = \varepsilon_r' - j\varepsilon''$ where the real term is referred to as the permittivity, and the imaginary term, the loss factor. Permittivity represents a materials ability to store electromagnetic energy, where loss factor represents a materials ability to absorb electromagnetic energy [7].

As it relates to the measurement technique for materials characterization, there are numerous methods that can be used [9],[10],[11]. The loaded transmission line approach is common for performing materials characterization. This is done by placing the material of interest within a transmission line (for example, a rectangular waveguide [7]) and measuring the reflection and transmission properties. These measurements are used in conjunction with an inverse recalculation routine to determine the dielectric properties. Another option is to use a short-circuited transmission line [6], where one end of a

rectangular waveguide is shorted, the sample is placed inside, and a one-port (reflection properties only) measurement is performed. For this work, due to restrictions related to the geopolymer materials, the short-circuited transmission line approach was used for measurements.

1.3. DIELECTRIC MIXING MODELS

Dielectric mixing models relate the dielectric properties of constituent materials (and their relative volume fractions) to those of an overall effective (or composite) material. Many models have been developed to describe different types of constituent mixtures [5]. These models consider the inclusion (i.e., any material with non-majority volume fraction) geometry, where mixed particles may be considered as spheres, needles, or disks depending on their natural form. For this work, due to the frequency bands of interest (and hence wavelengths on the order of centimeters), all inclusions are approximated as spherical for this work [5]. To this end, the power law mixing model will be used to relate the individual constituents to the overall (respective) properties.

1.4. CURRENT INVESTIGATION

As mentioned, this work applies the one-port loaded short circuit rectangular waveguide (SCRWG) method for materials characterization in order to better understand the geopolymer curing process, including the role of water in the same. This measurement technique is essential for the measurement of geopolymers, as the geopolymers are liquid when initially cast, making two port loaded rectangular waveguide measurements difficult, as liquid may leak from either port. Using a sealed

and shorted sample holder, liquid may be poured into the sample holder and the sample maintained for any needed length of time. Additionally, this work discusses the significance of sample placement within the sample holder. This work will employ a dielectric mixing model in order to approximate the dielectric properties of the geopolymers cast and cured as part of this work. These calculated dielectric properties will then serve as inputs to a full wave high frequency simulation model, which will determine the reflection properties of such a material when placed in a short-circuited waveguide sample holder. In this way, a comparison between measurement and simulation may be made.

This thesis consists of 5 sections, including the current. The second section considers the effect of sample placement, length, and dielectric properties on short circuit rectangular waveguide measurements of the same. The third section provides measurement results and subsequent analysis of geopolymer samples consisting of different sample lengths, mixture designs, and curing temperatures, measured at two different frequency bands. The measurements span a curing period of two hundred hours, and the temporal behavior of the results as it relates to sample length, geopolymer design, and curing temperature is studied. In section four, a dielectric mixing model is utilized in order to determine the overall dielectric properties of the geopolymer mix design, given the properties of the constituents. These properties are used as inputs for a full wave simulation, with the results compared to measured geopolymer reflection measurements from Section 3. The final section includes a comprehensive discussion of the conclusions of this work, relevant lessons learned, potential improvements, and future work.

2. MEASUREMENT APPROACH

2.1. MATERIALS CHARACTERIZATION

Microwave materials characterization is the process of experimentally determining the dielectric properties of a material. Dielectric properties are often referenced to free space as is the case here and are denoted as $\varepsilon_r = \varepsilon_r' - j\varepsilon''$, where the real term is the permittivity, and the imaginary term is the loss factor. These properties describe the ability of a material to store (via permittivity) and absorb (via loss factor) energy. These properties can be related to chemical and physical properties, material composition, etc., and as such, are useful in a number of fields [7], [8]. One such application for microwave materials characterization is that of geopolymer science, where during the curing process, water may change chemical state from bound to free, or vice versa [4]. Due to the sensitivity of water to microwave frequencies, measuring the dielectric properties of the geopolymer during the curing cycle may be used to detect changes in the curing process (specifically the chemical state of water) [4]. As microwave materials characterization is inherently experimental in nature, dielectric properties may be measured using a number of techniques.

2.2. MEASUREMENT TECHNIQUE

Dielectric properties are intrinsic, meaning they are independent of measurement technique. Because of this, many techniques for characterizing dielectric properties have been developed [9], [10]. One technique used to measure dielectric properties is the loaded transmission line approach [9], which is utilized in this work. Specifically, here, a

rectangular waveguide section is used as the transmission line which is herein referred to as the sample holder. Two port loaded waveguide measurements have been successfully applied previously for materials characterization measurements [7]. Such measurements are conducted by placing the sample in the waveguide sample holder, as is illustrated below in Figure 2.1, and connecting each end to a calibrated Vector Network Analyzer (VNA). In this way, calibrated transmission (S21) and reflection (S11) coefficient measurements may be made and subsequently used to determine dielectric properties [9].

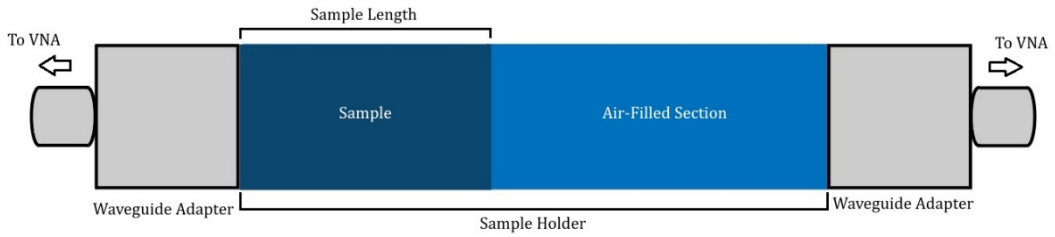

Figure 2.1: Diagram of a loaded rectangular waveguide containing a sample for two-port measurement.

The loaded transmission line approach has been used to successfully measure solid and granular materials [11]. However, measurement of liquids (while possible) is challenging due to the need to contain the sample within the holder. To this end, this challenge can be alleviated through the use of a short-circuited rectangular waveguide (SC-RWG) sample holder with subsequent one port measurements, as is illustrated in Figure 2.2. Such an approach is more conducive for liquids because there is only one open end, and the measurement can be conducted with the short-circuited line rotated 90º from the orientation shown below, effectively placing the open end that connects to the

VNA at the top, with the liquid sample flush again the SC end. In this way, the liquid can be better contained while maintaining proper geometric placement (e.g., surface areas of the sample at the ends are parallel to the surface area of the aperture of the WG at the end of the WG section).

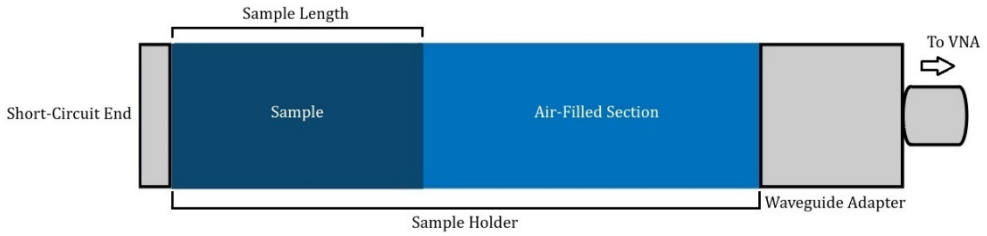

Figure 2.2: Diagram of a loaded rectangular waveguide containing a sample for short-circuited one port measurement.

This measurement technique, however, poses its own disadvantages. As it utilizes a one port measurement (vs. the two port above), there are fewer measured quantities (e.g., solely S11 vs. S11 and S21) and therefore, the iterative/root finding approach to calculate dielectric properties is more complicated [12]. As such, when possible, the two port approach for loaded transmission line measurements is preferred. However, if liquid measurements are necessary, the one port approach may be best overall.

As it relates to the goals of this work, a microwave materials characterization approach is applied to the study of geopolymer materials. As mentioned above, the role of water in the curing process is of particular interest. To this end, since geopolymer materials begin in a liquid phase and transition (cure) to a solid phase (during the curing process), two port measurements are not idea. As such, the remainder of this section

focuses on important aspects of a one port measurement of a loaded rectangular waveguide terminated in a short circuit that is intended for materials characterization.

2.3. SHORT-CIRCUITED LINE TECHNIQUE

The short circuit terminated transmission line method was introduced in [12]. In [12], a measurement limitation was proposed regarding the placement of the sample within the short-circuited line. This limitation arises due to boundary conditions brought about by the short-circuited end [13]. More specifically, when an electric field propagates in a short-circuited transmission line, it reflects at the short-circuited (SC) end. This creates forward and backward traveling waves, with the summation (i.e., total electric field at any point along the line) creating a standing wave as a function of line length. At the location of the short circuit, boundary conditions dictate that the total electric field must equal zero. As such, [12] states that rather than placing a sample at an electric field null, it must be shifted to a location of maximum electric field in order to accurately characterize the dielectric properties. This maximum is located at odd multiples of $\lambda_g/4$ from the SC end, where λ_g is the wavelength in the waveguide. In fact, [12] suggests that sample placement should be centered at $\lambda_g/4$ to ensure maximum interaction of the material with the electric field. These maximums and nulls that occur within a SC-RWG are illustrated in Figure 2.3, where the electric field in an air-filled ($\varepsilon_r = 1$) SC-RWG can be seen.

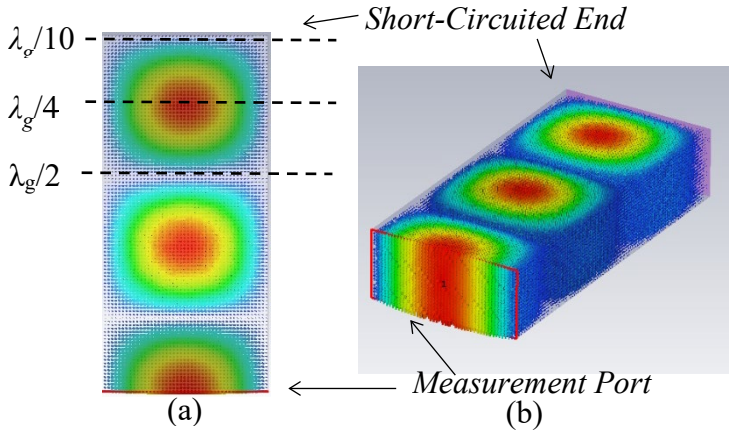

Figure 2.3: Top (a) and 3D (b) views of electric field in a SC-RWG [8].

As shown above, the electric field has maxima at odd multiples of $\lambda_g/4$ and minima (nulls) at even multiples of $\lambda_g/2$ along the length of the SC-RWG. At the sides of the waveguide, the electric field also exhibits a minimum, hence the circular electric field pattern visible is that of a dominant TE10 mode standing wave pattern. Figure 2.3 is useful because it illustrates regions where samples may be placed in order to ensure maximum interaction with the electric field. What is not clear in [12] is the effect of sample length and/or dielectric properties on the requirement of sample placement at an electric field maximum. In other words, samples of significant length (multiple wavelengths) will experience more maxima and minima than a shorter sample (less than $\lambda_g/4$), so sample placement may not be critical. The same may be true for materials with high dielectric properties. To this end, in this section, the effect of sample placement, length and dielectric properties will be examined via full wave simulation and measurement to better understand the measurement limitations that must be followed in practice.

2.4. SIMULATIONS

Full wave simulations were conducted using CST Microwave Studio™ to examine the effect of sample length, placement within the SC-RWG, and dielectric properties on the reflection properties of a sample placed within a SC-RWG sample holder. Simulations were conducted in the X-Band (8.2-12.4 GHz). At 10 GHz, the location of λ_g (in an air-filled SC-RWG) will be 4 cm.

2.4.1. Short Samples. First, simulations on short (defined as a length less than $\lambda_g/4$) samples were conducted. Beginning with a low permittivity and low loss sample ($\varepsilon_r = 2.6 - j0.001$), chosen to be representative of acrylic for comparison later with measurement, sample lengths between $\lambda_g/10$ and $\lambda_g/4$ were simulated, placed at the SC-end of the sample holder and centered at $\lambda_g/4$. The simulated magnitude of the complex reflection properties is displayed in Figure 2.4 below. The phase of the complex reflection properties is not explicitly studied, as the goal of this section (effect of sample placement, length, and dielectric properties) manifests directly in magnitude.

As seen below in Figure 2.4 it is clear that these simulations (for both placements) deviate only slightly from 0 dB, due to the low permittivity and loss factor. As |S11| from an empty SC-RWG sample holder will (ideally) be equal to 0 dB, it is clear from the above that the presence of all samples considered minimally affects the reflection properties. To this end, such a result is not a good candidate for materials characterization measurements as the signal interaction with the material (sample) is minimal.

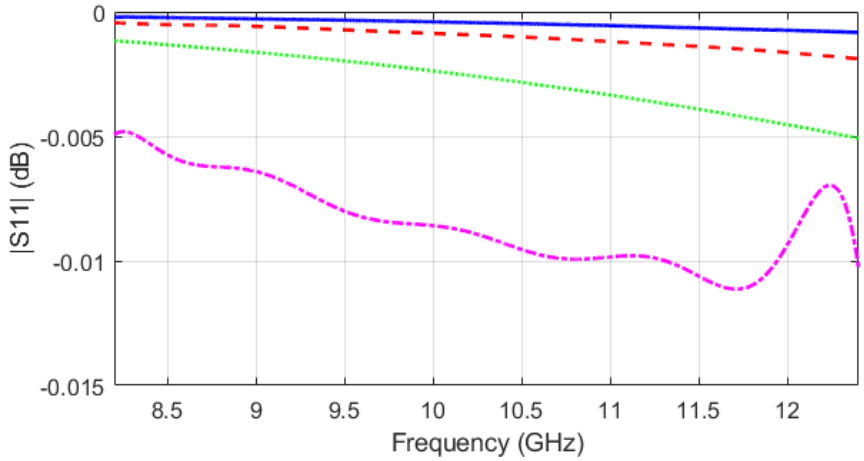

(a)

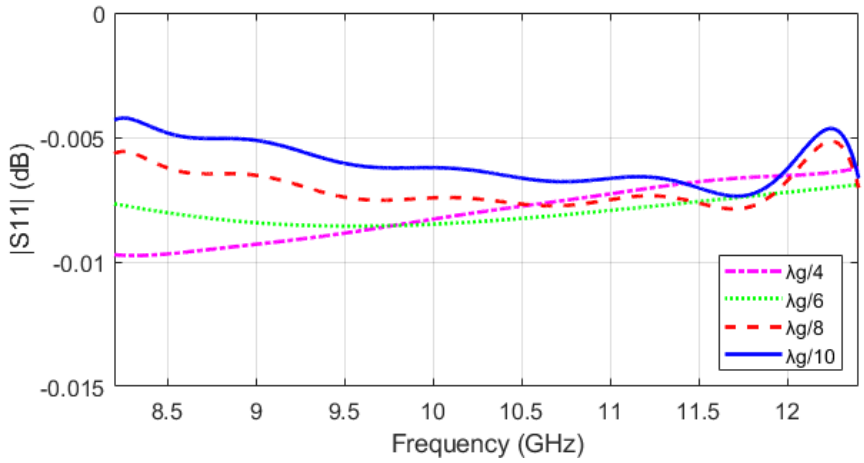

(b)

Figure 2.4: Simulated |S11| for short acrylic sample simulations placed at the SC end (a) and centered at $\lambda_g/4$ (b) [8].

When comparing the effect of sample placement specifically, Figure 2.4a shows that the samples placed against the SC end of the waveguide interact with the electric field less than those in Figure 2.4b, which are centered at $\lambda_g/4$, as |S11| is closer to 0 dB in those cases. It is also expected that the response differs as a function of sample placement, as sample placement affects the input impedance of the SC-RWG and hence

the reflection properties [10]. In addition and despite these differences in Figure 2.4a and Figure 2.4b, when the sample length exceeds $\lambda_g/6$, |S11| is noticeably different from an air-filled waveguide (e.g., 0 dB response) regardless of the sample's placement in the waveguide.

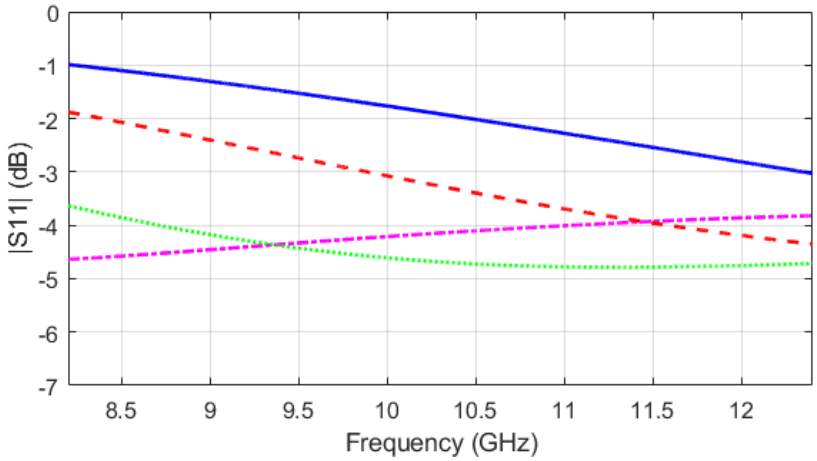

(a)

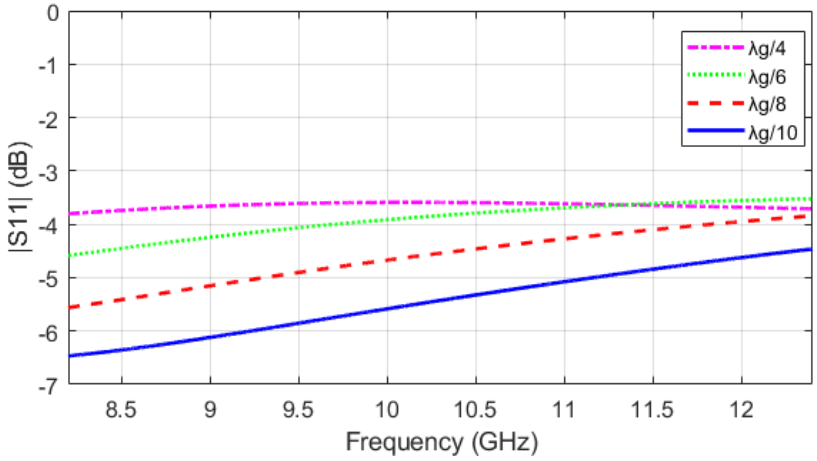

(b)

Figure 2.5: Simulated |S11| for short tap water samples placed at the shorted end (a) and centered at $\lambda_g/4$ (b) [8].

Simulations were also conducted considering a sample with dielectric properties of $\varepsilon_r = 5.11 - j13$ (selected to represent measured values for tap water, characterized using the calibrated two port rectangular waveguide measurement technique [8]). The simulation results are shown above in Figure 2.5. As mentioned, phase is not included in these simulations as the purpose is to evaluate how |S11| changes as a result of sample placement, length, and dielectric properties. The samples placed at the shorted end differ greatly from those of an air-filled waveguide (i.e., 0 dB). Even for the sample with a length of $\lambda_g/10$, a 1 dB reduction in |S11| is evident at 8.2 GHz, and approximately a 3 dB reduction in |S11| is shown at 12.4 GHz. The reflection properties of the samples centered at $\lambda_g/4$ also experience significant attenuation (on the order of 4 dB). This is important, as it shows samples with greater dielectric constant and loss factor can be placed anywhere within the sample holder and still have a reliable measurement, regardless of sample length. This is quite important as it relates to ease of sample placement and subsequent measurement, particularly if a liquid is to be measured.

2.4.2. Long Samples. Samples with longer lengths ($\lambda_g/3$ and $3\lambda_g/4$) were also considered via simulation. As above, the effect of placement within the SC-RWG sample holder as well as dielectric properties on |S11| was investigated. To begin, results for an acrylic sample ($\varepsilon_r = 2.6 - j0.001$,) located at the SC end and centered at $\lambda_g/4$ are shown in Figure 2.6. Also included are the results for a sample of length $\lambda_g/4$ (from above) for comparison.

As seen, |S11| of Figure 2.6a and Figure 2.6b for all 3 sample lengths is quite similar, with a reduction of |S11| on the order of 0.01 – 0.03 dB for all, even though their respective placement within the SC-RWG differs. This similarity in response can be

explained by considering the electric field within the SC-RWG for each case, as is shown in Figure 2.7. Here, the purple shaded region represents the location of the sample, and the multi-colored region shows the electric field, with the maxima represented in red.

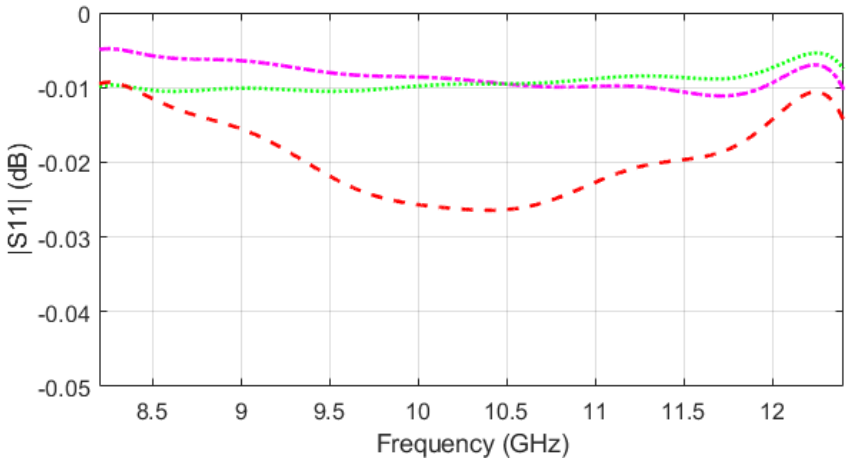

(a)

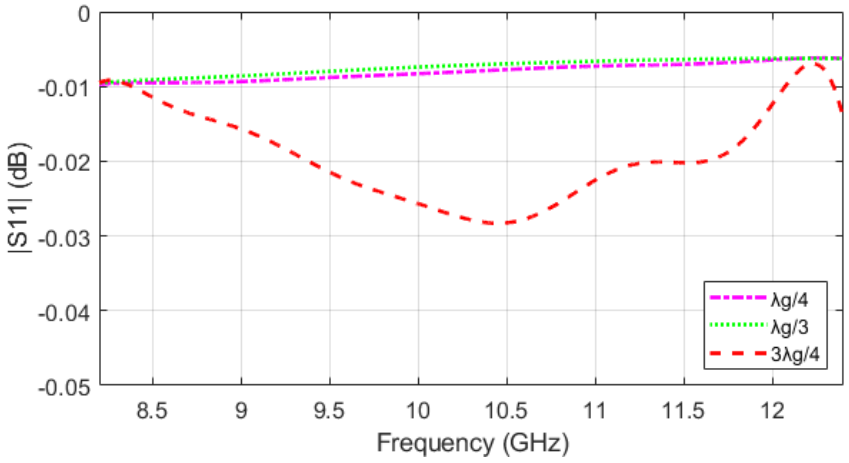

(b)

Figure 2.6: Simulated |S11| for long acrylic samples placed at the shorted end (a) and centered at $\lambda_g/4$ (b) [8].

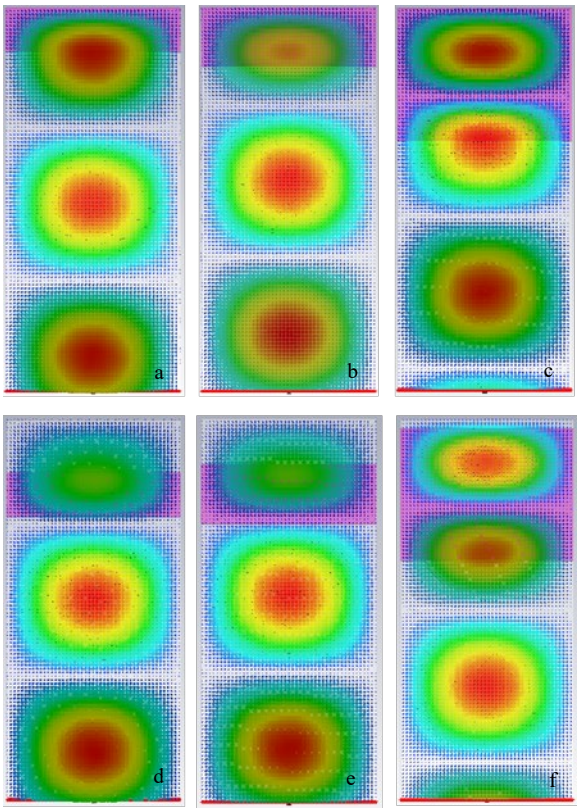

Figure 2.7: Simulated electric field in a SC waveguide filled with acrylic samples of lengths $\lambda_g/4$, $\lambda_g/3$, and $3\lambda_g/4$ placed at the shorted end (a, b, and c, respectively) and centered at $\lambda_g/4$ (d, e, and f, respectively) [8].

For all results shown in Figure 2.7 (a-f), the effect of the sample (due to dielectric boundary conditions [9], [10]) on the electric field pattern is evident through the changes on the electric field distribution over the full length of the SC-RWG. This is true for flush and shifted samples. In addition, when considering the electric field distributions to the corresponding |S11|, it can also be seen that in Figure 2.7a-b, the field distribution is similar, as is the case for the same samples' |S11| of Figure 2.7a. Similarly, Figure 2.7c differs from Figure 2.7a-b, as is also the case for the respective results of Figure 2.6a. The same trends are evident for the field distributions of Figure 2.7d-f when considered with the results of Figure 2.6 b. Overall, it can be concluded that for low dielectric property

materials, the sample length should be greater than (but not equal to) integer multiples of $\lambda_g/2$ for materials characterization measurements, regardless of sample placement. (Note, sample lengths of integer multiples of $\lambda_g/2$ should be avoided in order to avoid half-wave transformer effects [7], [8] if single frequency characterization is of interest).

Simulations for samples of tap water (high permittivity and loss factor) at lengths of $\lambda_g/4$, $\lambda_g/3$, and 3 $\lambda_g/4$ were also conducted to determine |S11| and the electric field distribution, as above. The results for the same are shown in Figure 2.8 (|S11|) and Figure 2.9 (electric field distribution).

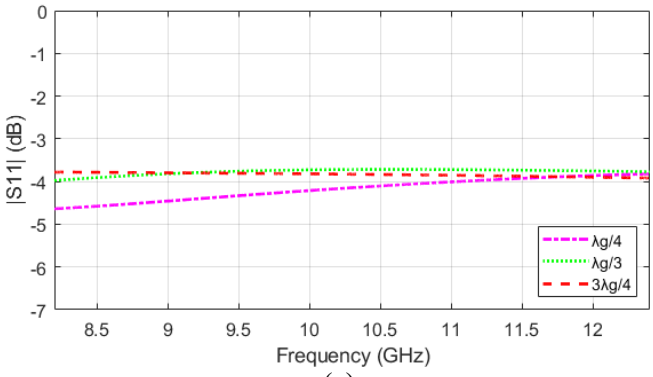

(a)

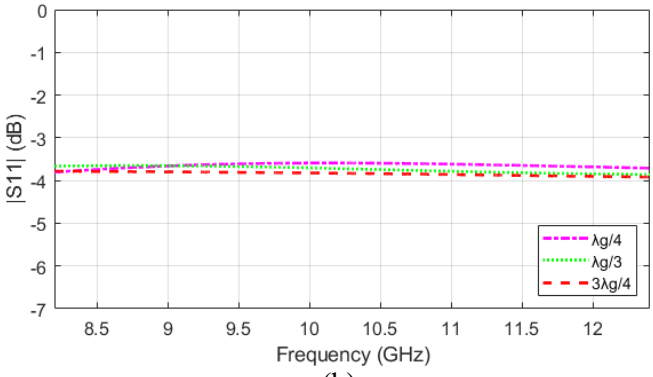

(b)

Figure 2.8: Simulated |S11| for long tap water samples of length $\lambda_g/4$ and greater, placed next to the shorted end, (a) and centered at $\lambda_g/4$ (b) [8].

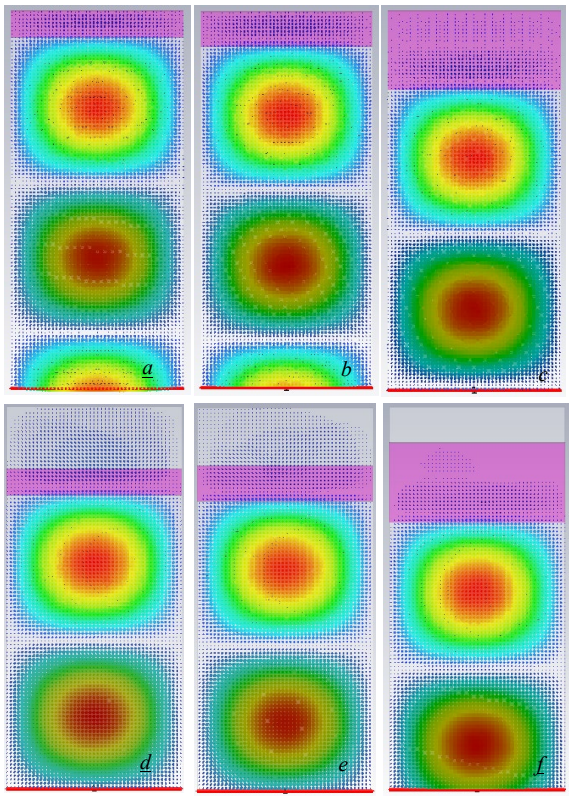

Figure 2.9: Simulated electric field in a SC waveguide filled with tap water samples of lengths $\lambda_g/4$, $\lambda_g/3$, and $3\lambda_g/4$ placed at the shorted end (a, b, and c) and centered at $\lambda_g/4$ (d, e, and f) [8].

As seen, |S11| for all three sample lengths and both placements are similar, with no more than ~0.8 dB variation amongst all. The length of samples (illustrated in Figure 2.9) also appears physically shorter than the acrylic samples above. This is a result of the greater permittivity of the water, resulting in a shorter wavelength and hence physically shorter samples. Another interesting aspect to note in Figure 2.9 is the fact that in all cases, the field magnitude within the water samples is much less than that in the empty RWG. In addition, the distribution looks very similar from one sample to the next, albeit shifted commensurate with the sample length. This is due to the fact that the high permittivity and loss factor (through the dielectric boundary conditions [9]) caused most

of the electric field incident on the sample to be reflected. In this way, the field distribution looks similar to that of an empty SC-RWG (Figure 2.3). Overall, these results support the conclusion that for high permittivity and loss factor materials, sample length and placement is not critical for materials characterization measurements, thereby removing the restriction originally stated in [7] that materials must be placed within the SC-RWG sample holder at a location of electric field maximum.

2.5. MEASUREMENTS

To verify the conclusions deduced from the simulated results above, measurements were performed in a SC-RWG sample holder on acrylic and water samples at X-Band. Acrylic sample lengths of 2 mm (~0.1 λ_g at 10 GHz in air) were chosen to represent 'short' samples, and sample lengths of 2 cm (~λ_g at 10 GHz in air) were chosen for 'long' samples. It should be noted that the long sample is an integer multiple of $\lambda_g/2$ at 10 GHz specifically, but since these measurements are over the full X-band, the measurement concern of samples of this length is alleviated. Both samples were placed at the shorted end of a RWG sample holder and centered at a distance of $\lambda_g/4$. A calibrated Anritsu MS4644A Vector Network Analyzer was used to measure |S11| as illustrated above in Figure 2.2. In order to achieve the shifted measurement, a section of foam with a length of 10 mm (~ $\lambda_g/4$ at 10 GHz in air), was placed flush with the short-circuited end and the sample itself placed flush against the foam. In this way, the intended sample placement in the sample holder was achieved. Foam has measured dielectric properties of 1 – j 0.07 as per [10] (measured using a calibrated two-port loaded transmission line

approach). The dielectric properties of foam are close to the properties of air, meaning its presence will minimally affect the results.

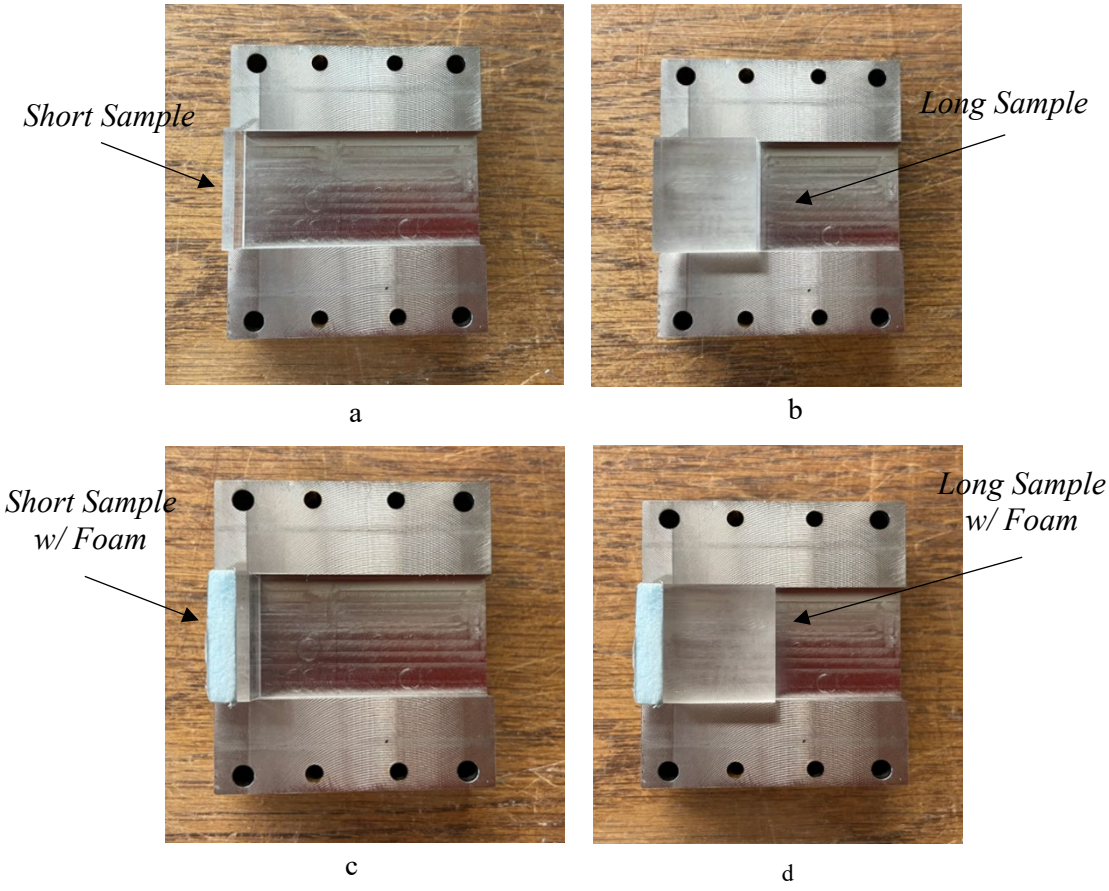

Figure 2.10: Unshifted acrylic samples $0.1\ \lambda_g$ (a), λ_g (b), and shifted acrylic samples with blue foam inserts $0.1\ \lambda_g$ (c), λ_g (d).

In Figure 2.10, shown above, photographs of the loaded SC-RWG sample holder are shown including the short and long acrylic samples. The foam is also evident for the shifted samples. In Figure 2.11, shown below, photographs are shown of this sample holder connected to a waveguide to illustrate how these sample holders are used in measurement.

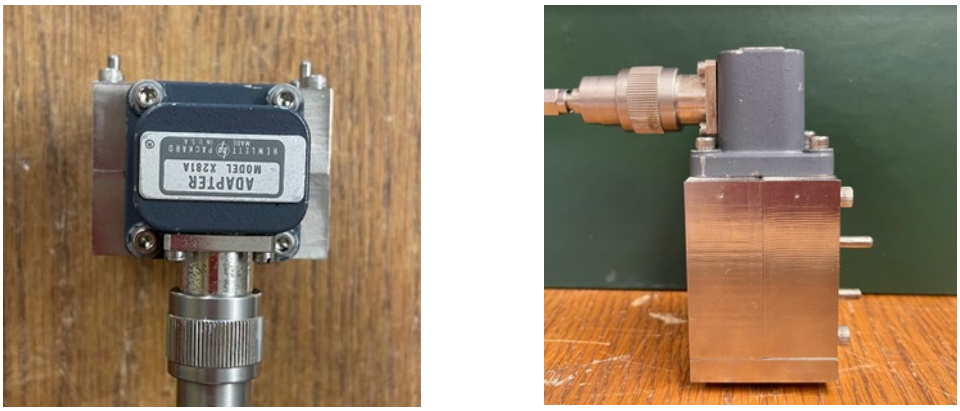

Figure 2.11: Top and side view of sample holder connected to an X-Band waveguide adapter for measurement.

The measurement and simulation results (both |S11| and phase, to show agreement between measurement and simulation) for the thin acrylic samples placed at the short circuit end and shifted to $\lambda_g/4$ are shown next in Figure 2.12. As can be seen, the simulated and measured results have similar trends in |S11| as a function of frequency but not in value. This is attributed to an error in the estimated/calculated dielectric properties used for the simulation (particularly loss factor). Furthermore, the measured phase contains much more variation as a function of frequency than the simulated of the same. This is attributed to a longer electrical length of the simulated samples as compared to the physical measured samples. This is directly a result of a difference in permittivity between what was used for simulation and that of the physical samples. The addition of foam, while assumed to be negligible (as noted above) may have also affected the measured results (particularly in |S11| through additional and un-accounted for signal loss). Overall and as was also noted above, while [7] suggests that sample lengths of even multiples of $\lambda_g/4$ should be avoided, Figure 2.12 supports the conclusion that short

samples of low dielectric properties must be strategically placed in the SC-RWG sample holder, while longer samples do not have this restriction.

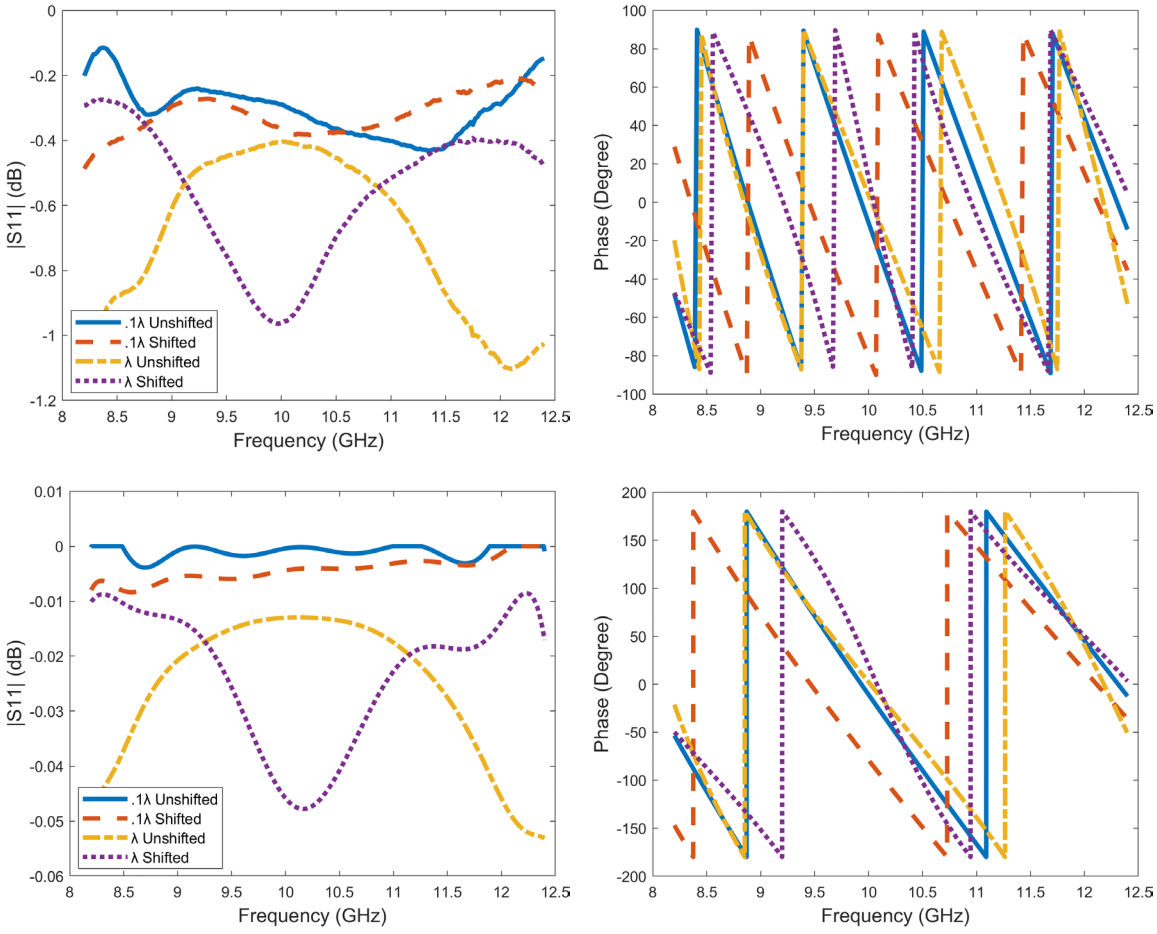

Figure 2.12: |S11| and phase for measured (top) and simulated (bottom) acrylic samples [8].

Lastly, similar measurements were conducted for tap water, with |S11| and phase shown below in Figure 2.13. However, unlike above, measurements were only performed on a sample of length $3\lambda_g/4$ due to complexity in sample preparation. In other words, preparing a thin (e.g., length shorter than $\lambda_g/4$ or less than ~3 mm) liquid sample was difficult to do reliably and with confidence. As seen, |S11| is similar in trend as a function

of frequency, albeit with different values. This is attributed to error in the loss factor assumed in simulation. Similar to the above, the variation in phase is greater as a function of frequency for the measured results, indicating a longer electrical length (and hence higher permittivity than that assumed in simulation).

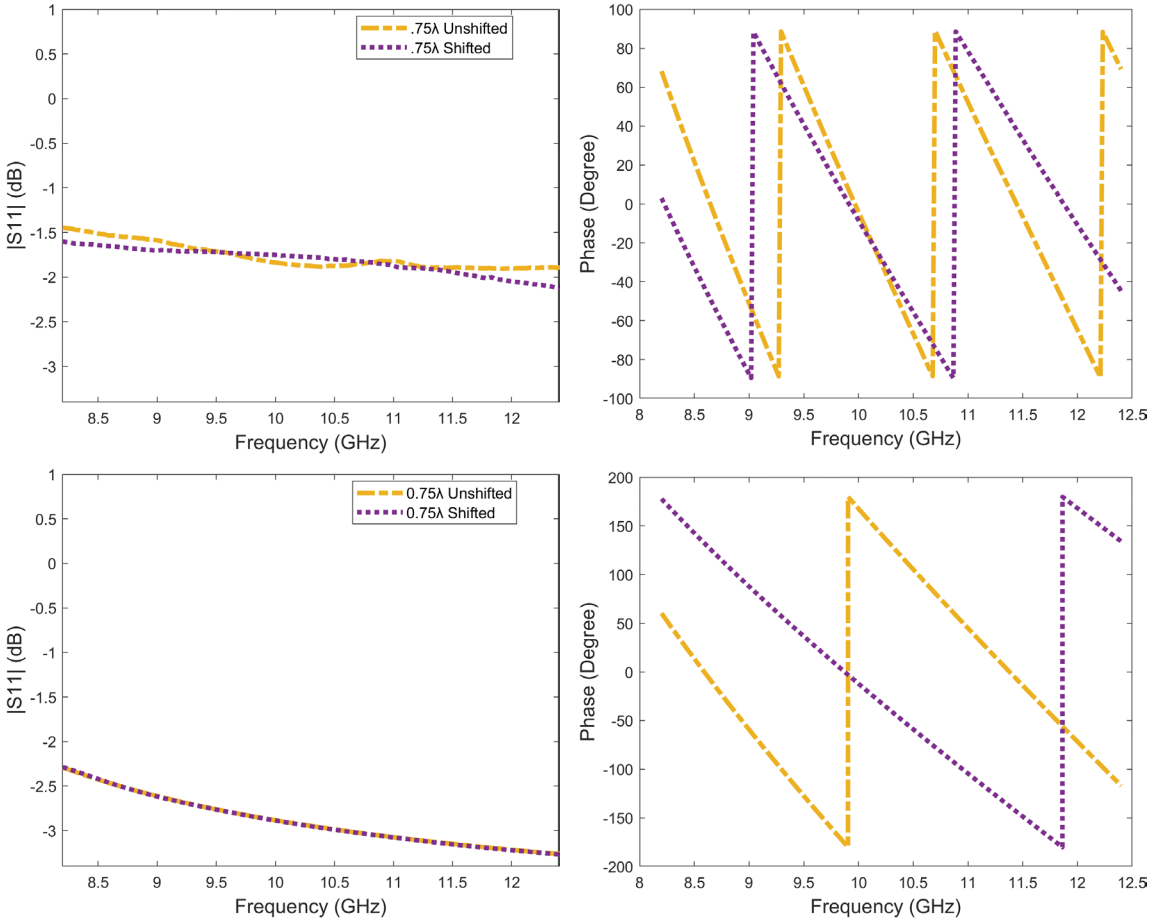

Figure 2.13: Magnitude and phase for measured (top) and simulated (bottom) water samples [8].

2.6. CONCLUSION

Overall, materials characterization measurements can be performed reliably regardless of the sample placement within a SC-RWG sample holder if the sample length is greater than $\lambda_g/6$, as has been shown through both simulation and measurement for both low and high permittivity and loss factor materials. For low permittivity and loss factor materials, the sample must be shifted to a location of electrical field maximum, nominally $\lambda_g/4$. For high permittivity and loss factor samples, the samples may remain flush with the SC-end (an important point as it relates to ease of measurement, particularly for liquid materials).

3. GEOPOLYMER MEASUREMENT AND MATERIALS CHARACTERIZATION

3.1. GEOPOLYMER BACKGROUND

Geopolymers, or alkali activated materials, are a potential alternative to Ordinary Portland Cement (OPC) concrete. These materials can provide a durable and carbon friendly alternative to traditional OPC [14],[15]. They are produced by mixing an aluminosilicate powder with an alkaline solution. In this work, several geopolymer mixtures were cast in short-circuited rectangular waveguide (SC-RWG) sample holders with subsequent high frequency reflection measurements conducted throughout the curing cycle. Two geopolymer mixtures were considered; one consisted of metakaolin powder mixed with sodium silicate and deionized (DI) water and the other, metakaolin powder, sodium hydroxide and DI water. Once cast and over the course of the reaction/curing process, free water (i.e., H_2O) is produced. In typical OPC concrete, free water is added as a constituent, and it changes from a free state to a bound state during the cure cycle. In these geopolymer mixtures and in addition to the DI water, water is initially (pre-mixing) bound within the activator solution (an alkali solution which, when added to an aluminosilicate or calcium powder, forms a geopolymer). During the chemical process that takes place during curing, this water changes from a bound state to a free state. In other words, the reaction produces free water [16]. This chemical (curing) reaction and the effects of the same on relevant properties including structural properties are not well understood for geopolymer materials. This lack of understanding limits the ability of such materials to be implemented in modern-day construction. As it relates to this goal of this work, the role of water in the geopolymer reaction is something that can

be studied via microwave materials characterization, as the presence of free and bound water have been shown to impact high frequency measurements [4],[17],[18]. To this end, this section reports on the casting and subsequent high frequency measurements conducted on a set of geopolymer samples.

3.2. SAMPLE PREPARATION

Two geopolymer mixtures were synthesized and cast into sample holders, with regular high frequency complex reflection measurements conducted at S-Band (2.6-3.95 GHz) and R-Band (1.7-2.6 GHz) over the course of several weeks. Sample sets from both mixtures were stored in ambient conditions and in an oven (Quincy Labs 31-350ERS) set to 60 ºC (except when the samples were removed for measurement).

3.2.1. Geopolymer Sample Holders. The mixtures were cast into sample holders with cross-sectional dimensions corresponding to S-Band (2.84” x 1.34”) and R-Band (4.3” x 2.15”) waveguides. Twelve sample holders were made, six for R-Band, and six for S-Band. For the S-Band sample holders, there were two sample holders with a length of 3.7 cm, and four sample holders with a length of 2.6 cm. For the R-Band sample holders, there were two sample holders with a length of 5.2 cm, and four with lengths of 3.4 cm. Different lengths were chosen for each set to provide diversity of sample length in measurement. The sample holders were made with teflon lids containing rubber gaskets in order to seal moisture within the sample holders (i.e., to keep the free water present in the sample throughout the curing process). They are able to be dismantled and reassembled for easy cleaning, with gaskets at each joint in order to ensure no loss (evaporation) of free water. The sample holders were labeled A through F, with letters

‘A’ and ‘D’ being the longer sample holders. To illustrate, a photograph of three sample holders with lids are shown below in Figure 3.1. In addition, a photograph of two disassembled S-Band and R-Band sample holders is shown in Figure 3.2. The lids can be seen along with accompanying hardware used to secure the lids.

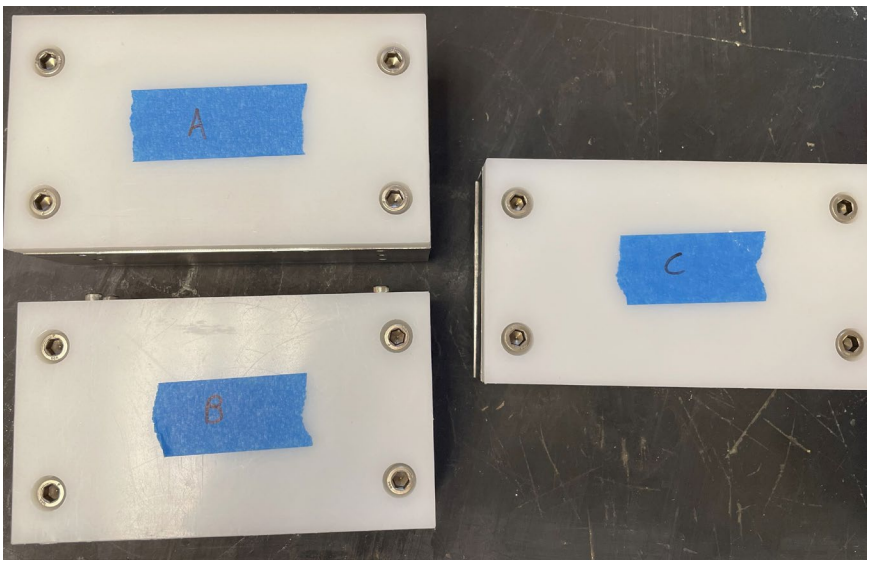

Figure 3.1: Three S-Band sample holders with lids.

3.2.2. Geopolymer Mix. When cast, each sample holder was intended to be completely filled (i.e., no air-filled section remains). To this end, the total volume needed to fill the three R-Band sample holders is 719.4 cm^3, and for S-Band 217.88 cm^3. To ensure enough material is mixed to completely fill all 6 sample holders, 750 cm^3 of geopolymer was made for the R-Band sample holders, and 250 cm^3 for the S-Band sample holders. For the R-Band material, 600 g of metakaolin, 525 g of DI water, and 176 g of a sodium hydroxide (referred to as Na-0) solution or 257 g of a sodium silicate (Na-2) solution was required in order to produce 750 cm^3 of geopolymer. For S-Band,

200 g of metakaolin, 175 g of DI water, and 59 g or 86 g of Na-0 or Na-2, respectively, was required. In total, 8 batches were made (varying frequency band, chemical composition, and storage temperature), as is summarized in Table 3.1.

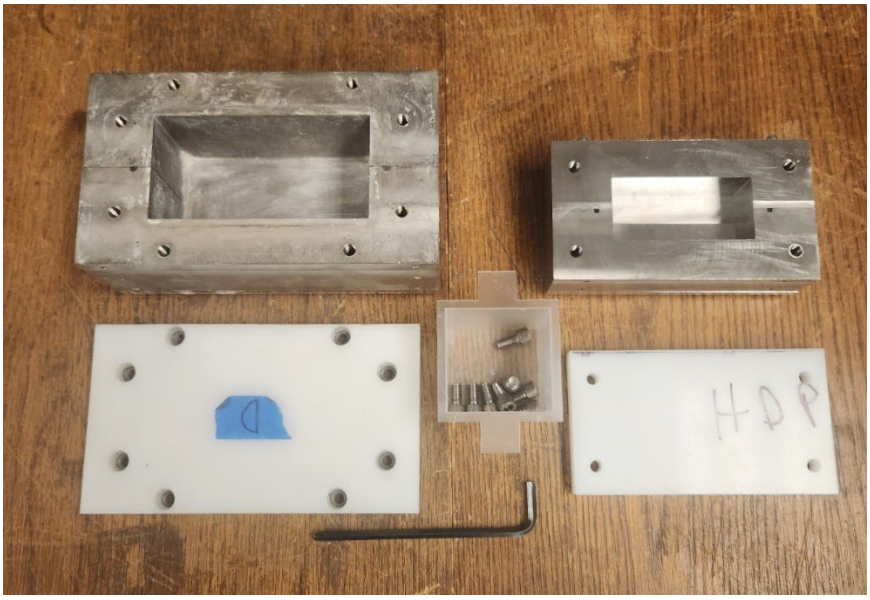

Figure 3.2: Empty, disassembled R-Band (left) and S-Band (right) sample holders.

3.2.3. Casting Process. To prepare a given batch, the mass of each constituent was measured. Then, all constituents were combined into a stainless-steel mixing bowl, and the mixture combined with a countertop stand mixer. The materials were mixed until the mixture is smooth and all ingredients are combined. A thin coating of WD-40 was applied to the inside of all sample holders prior to casting in order to ensure the sample does not bond to the holder during curing. After mixing, each sample holder was filled approximately half full of geopolymer material. Then, the sample holders were tamped and vibrated (by hand) in order to remove as much air (void content) from the material as possible. After the excess air content was removed, the sample holder was filled in full,

and the tamp/vibrate process repeated. A photograph of a filled sample holder is shown in Figure 3.3 below. After filling and tamping, the sample holders were sealed with the teflon lids, as shown in Figure 3.1 above.

Table 3.1: Batch Information

Batch Number	Band	Alkaline Solution	Storage Temperature
1	S	Na-0	Ambient
2	R	Na-0	Ambient
3	S	Na-0	60 °C
4	R	Na-0	60 °C
5	S	Na-2	Ambient
6	S	Na-2	60 °C
7	R	Na-2	Ambient
8	R	Na-2	60 °C

Depending on the batch, as per Table 3.1, the sample holders remained in ambient conditions or were placed in an oven at 60 ºC. It should also be noted that overall, the samples had less than 3 mm of unintended air gap after filling, tamping, and vibrating. To this end, the samples are considered full and the air gap ignored.

Figure 3.3: A filled S-Band sample holder.

3.3. MEASUREMENT PROCEDURE

One port complex (i.e., magnitude and phase) reflection measurements were conducted on each sample by connecting a calibrated port of an MS4644A Anritsu Vector Network Analyzer (VNA) to each sample holder. Shown below in Figure 3.4 is a diagram of a general SC-RWG measurement setup (including an air-filled section, which was minimized for the measurements in this work, with a maximum of 3 mm and therefore assumed to be zero). Once cast, measurements were taken every two hours for the first 8-10 hours in order to capture the changes in material properties (due to early-stage curing) in the hours immediately after mixing. In the following days and weeks, the measurement frequency decreased as the temporal change of the measured data reduced.

The mass of each (filled) sample holder is recorded before and after each measurement conducted throughout the curing cycle. Any decrease in mass is attributed to free water that evaporated during measurement while the sample was exposed to air.

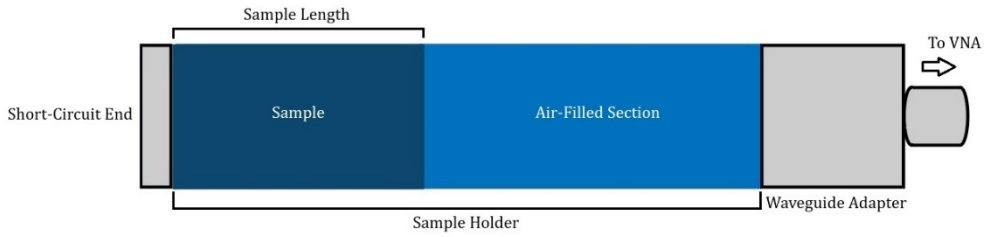

Figure 3.4: Diagram of a one-port measurement setup using a SC-RWG.

3.4. MEASUREMENT RESULTS

3.4.1. Mass Measurements. As mentioned, the mass of each filled sample holder was measured (pre- and post- measurement) over time. To this end, Table 3.2 shows the total mass lost over the course of curing for each S-band batch. In addition, Figures 3.5 - 3.8 show the mass measurements over the curing cycle for the batches noted in Table 3.2.

Table 3.2: S-Band Mass Measurement Results Characteristics

Batch Number	Curing Temperature	Geopolymer Design	Total Mass Lost (g)	Figure Number
1	Ambient	Na-0	~0.5	Figure 3.5
3	60° C	Na-0	~10	Figure 3.6
5	Ambient	Na-2	~5	Figure 3.7
6	60° C	Na-2	~20	Figure 3.8

As can be seen in Table 3.2 and each respective figure below, the mass of each sample decreases over the course of the measurement period. This decrease is important as it represents the lost (evaporated) free water over the course of the measurement period. It can also be seen that the mass in some samples also exhibits small positive and negative variations in magnitude over time. These variations are not representative of physical changes but rather, are attributed to the measurement error due to the scale used.

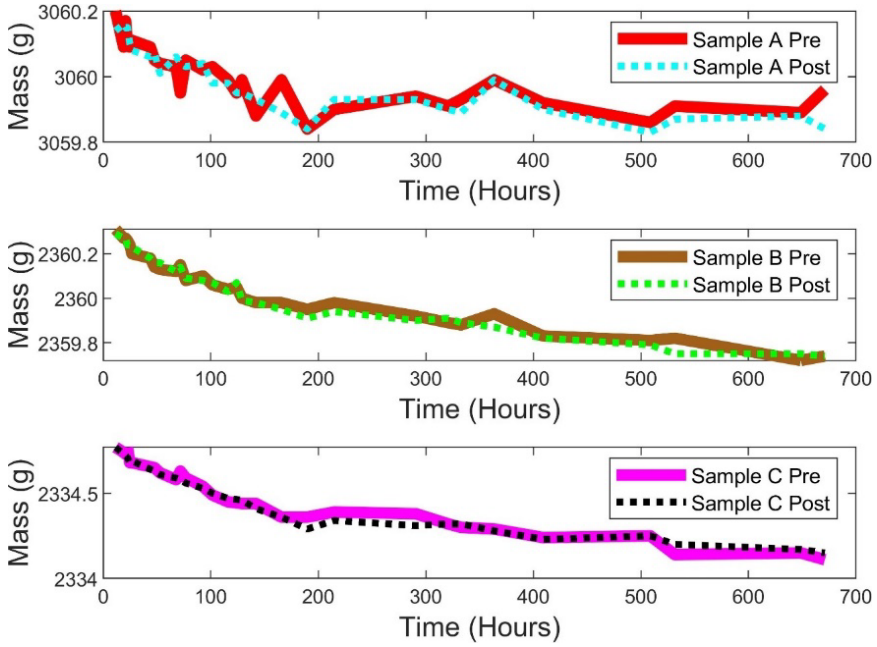

Figure 3.5: Mass as a function of measurement time for Batch 1, Samples A, B, and C, pre- and post-measurement, stored at ambient temperature.

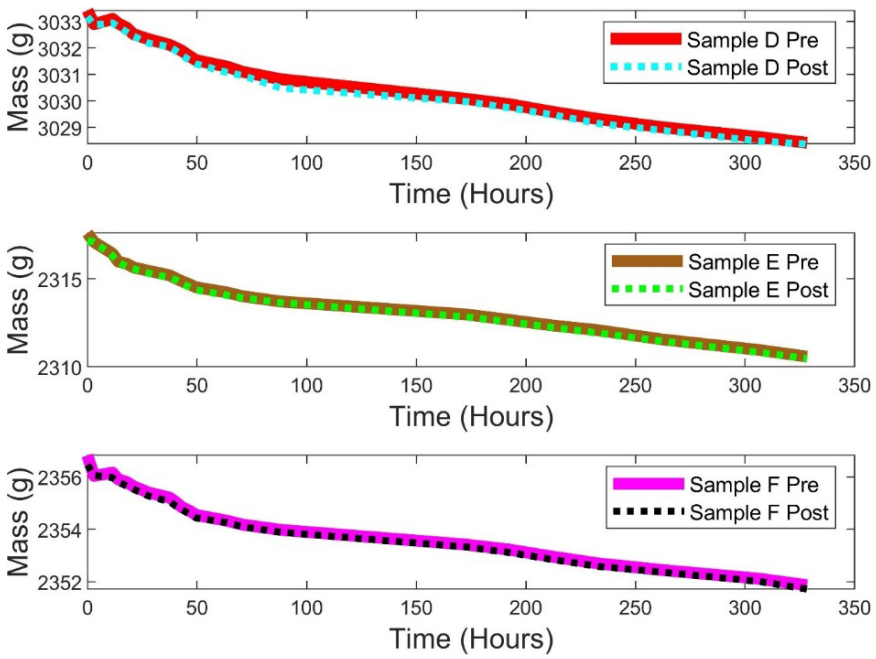

Figure 3.6: Mass as a function of measurement time for Batch 3, Samples A, B, and C, pre- and post-measurement, stored at ambient temperature.

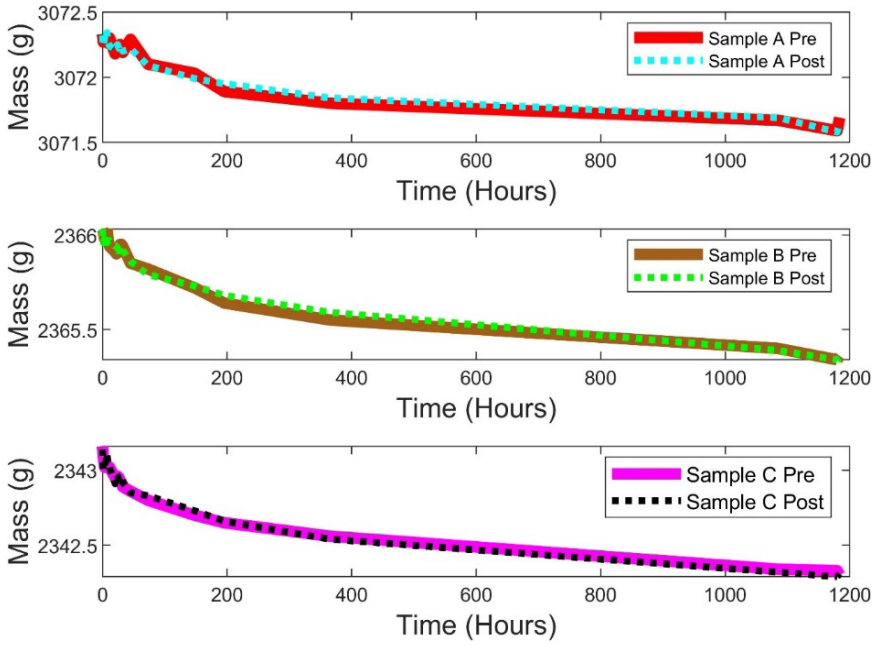

Figure 3.7: Mass as a function of measurement time for Batch 5, Samples A, B, and C, pre- and post-measurement, stored at 60 C.

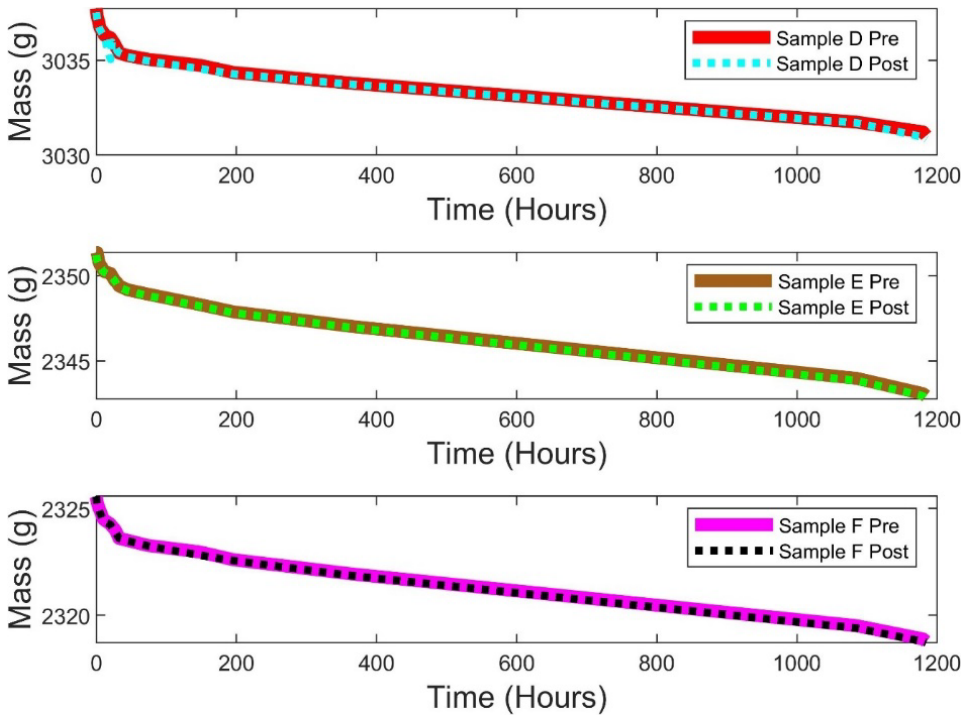

Figure 3.8: Mass as a function of measurement time for Batch 6, Samples D, E, and F, pre- and post-measurement, stored at 60 C.

In addition, Table 3.2 shows that the samples stored at 60 C lost more mass over time than those that cured in ambient conditions. Next, Table 3.3 contains the design and storage information for each R-Band sample and the total mass lost over the measurement period. Following the Table are Figures 3.9 – 3.12 which show the change in mass over the measurement period for the batches featured in Table 3.3.

As shown in Figure 3.12 and Figures 3.9-3.11, the samples of each batch decrease in mass over the course of the measurement period, and also that there are periods over the measurement period where the mass appears constant.

Table 3.3: R-Band Mass Measurement Results Characteristics

Batch Number	Curing Temperature	Geopolymer Design	Total Mass lost (g)	Figure Number
2	Ambient	Na-0	~1	Figure 3.9
4	60° C	Na-0	~6	Figure 3.10
7	Ambient	Na-2	~10	Figure 3.11
8	60° C	Na-2	~10	Figure 3.12

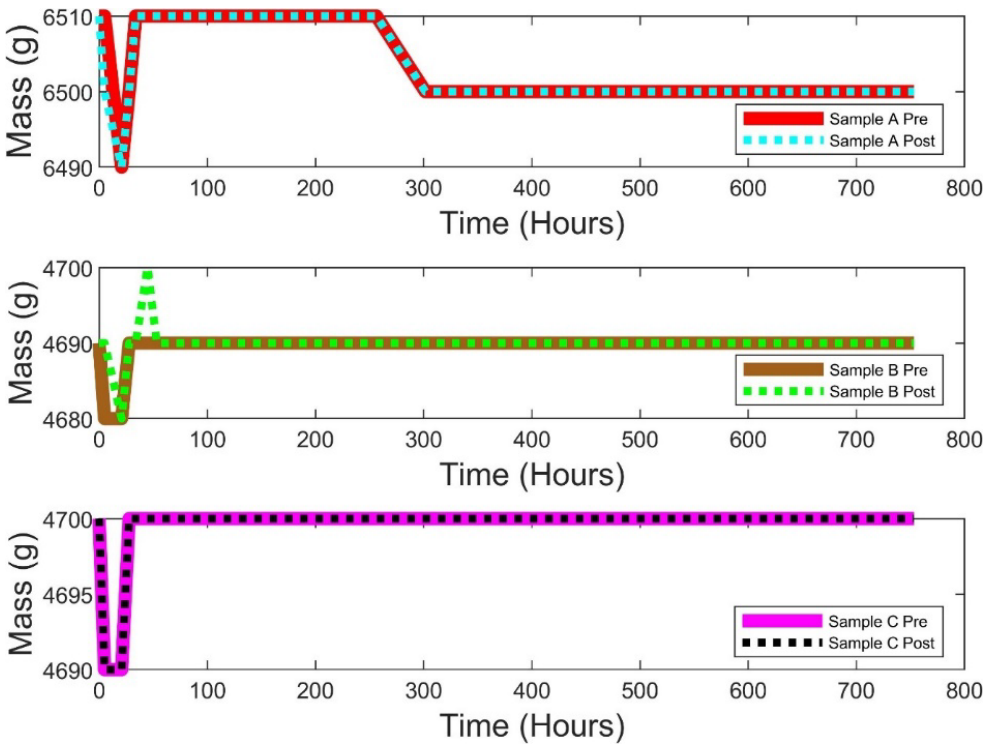

Figure 3.9: Mass as a function of measurement time for Batch 2, Samples A, B, and C, pre- and post-measurement, stored at ambient temperature.

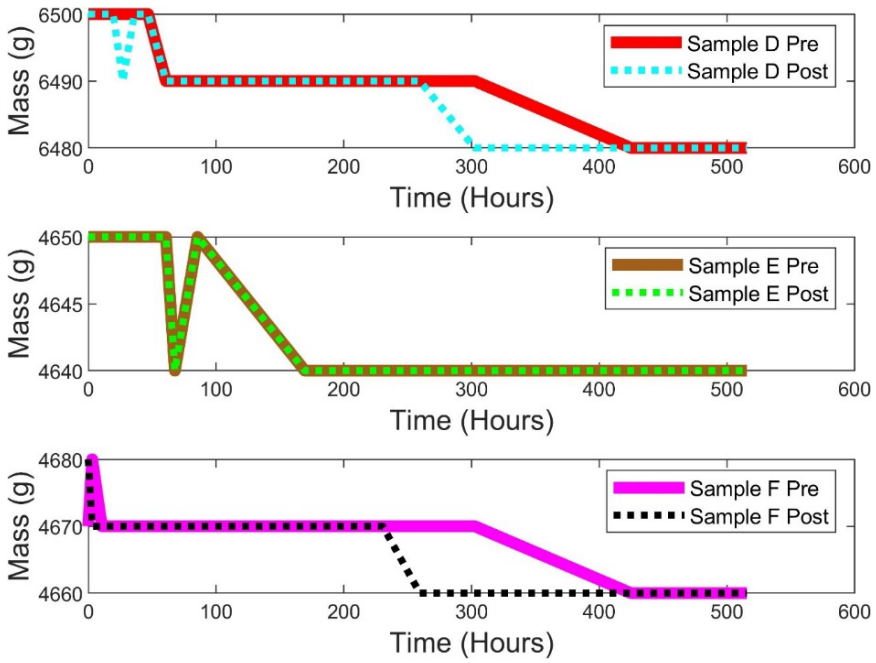

Figure 3.10: Mass as a function of measurement time for Batch 4, Samples D, E, and F, pre- and post-measurement, stored at 60 C.

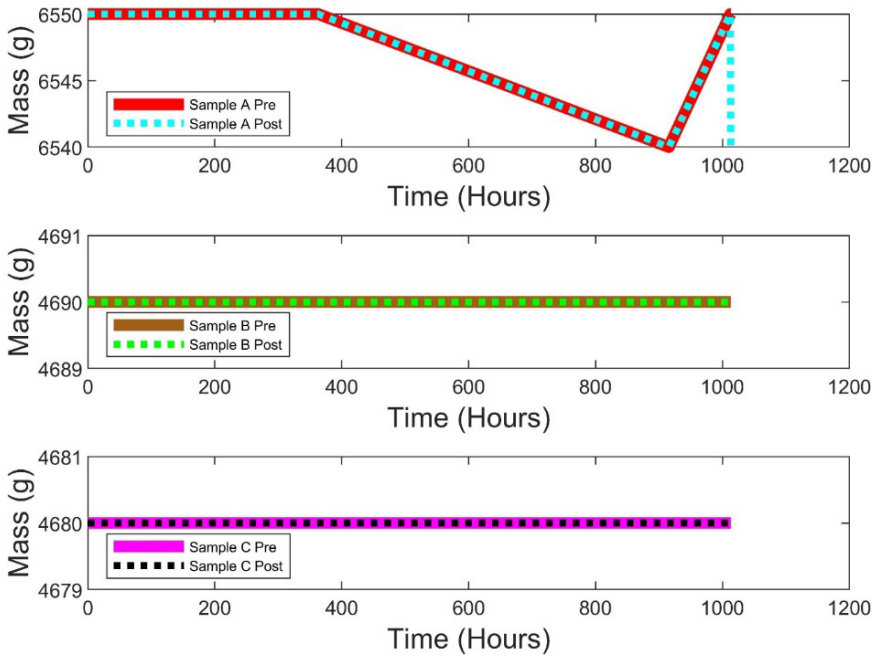

Figure 3.11: Mass as a function of measurement time for Batch 7, Samples A, B, and C, pre- and post-measurement, stored at ambient temperature.

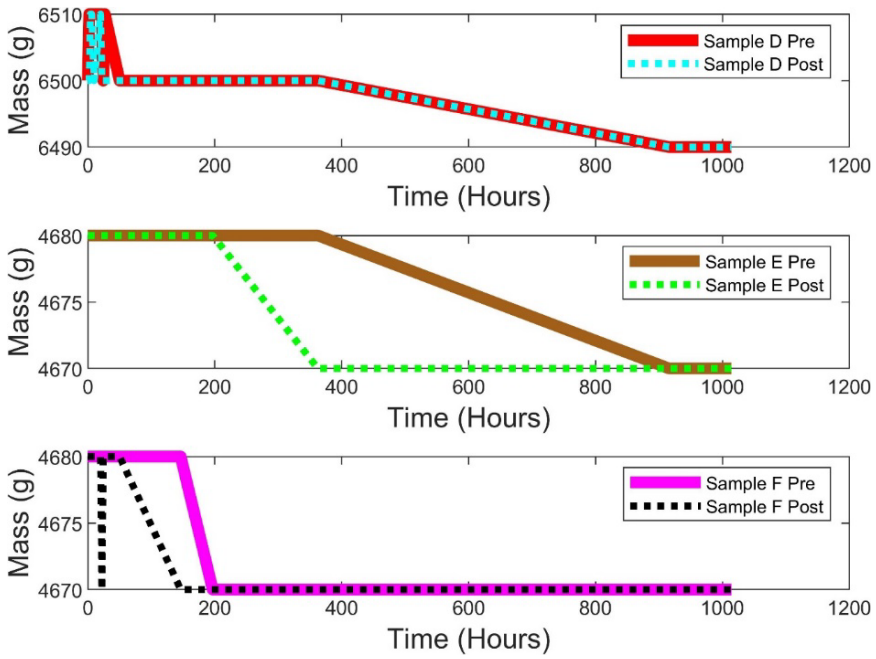

Figure 3.12: Mass as a function of measurement time for Batch 8, Samples D, E, and F, pre- and post-measurement, stored at 60 C.

This behavior was not evident above for the S-band samples. The reason for this is the scale that was used to measure S-band sample mass was not capable of measuring R-band sample mass. To this end, a different scale (from that used with the S-band samples) with a reduced accuracy (+/-10 grams) but larger range was used. Due to this reduced accuracy, small changes in mass are not noticeable, and some changes in mass may be exaggerated. The reduced accuracy of the scale also explains the apparent rapid changes in mass visible in Figure 3.9-3.12 (not representative of what actually occurs during curing but rather what can be measured). In addition and similar to the samples measured at S-Band, the batches cured at 60 C lost more mass than those stored at ambient.

3.4.2. Microwave Measurements. As mentioned above, calibrated one port microwave measurements were conducted with an Anritsu MS4644A Vector Network Analyzer throughout the curing cycle for each sample cast.

3.4.2.1. Na-0 samples. In Figure 3.13 below, the complex reflection properties (e.g., |S11| and phase) of Batch 1 (Na-0 design, ambient temperature, S-Band), beginning immediately after casting, are shown at 3 GHz as a function of curing time. As shown in Figure 3.13a below, as time progresses, |S11| decreases over the course of the measurement period for all samples. This means that temporally, the chemical processes that take place during curing are changing the electromagnetic properties of the material. Specifically, the material absorbs more energy as it cures and hence less signal returns and the reflection properties reduce. It can also be seen that the slope approaches zero at ~400 hrs, meaning the chemical reactions have likely ceased (or the effects on the reflection properties are no longer measurable) by this point.

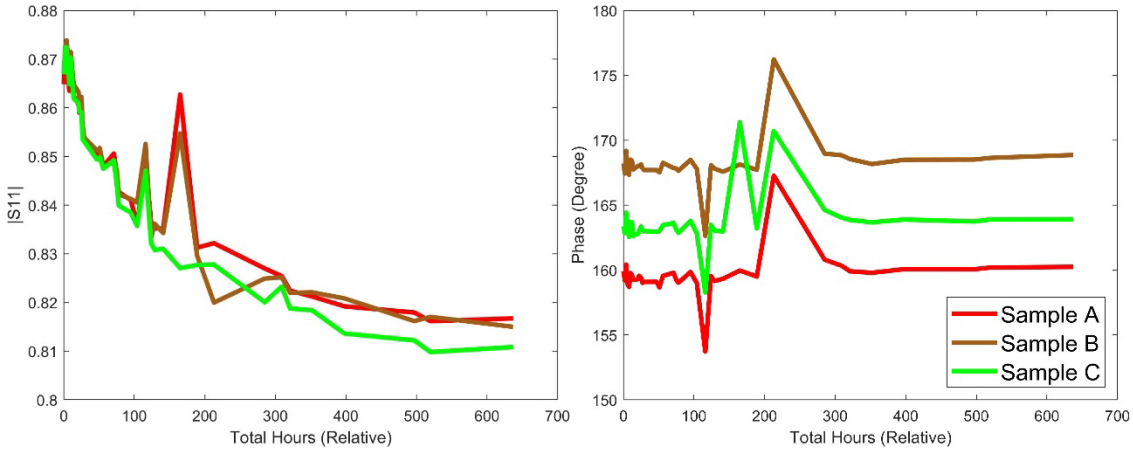

(a) (b)

Figure 3.13: Temporal |S11| (a) and phase (b) of Batch 1, Samples A, B, and C.

Phase (Figure 3.13b) shows almost no temporal variation over the course of the measurement period, aside from occasional large variations (also evident in |S11|) between 100 and 300 hours. This variation is attributed to measurement error (calibration, misalignment of the waveguide adapter, etc.) and is not attributed to material changes.

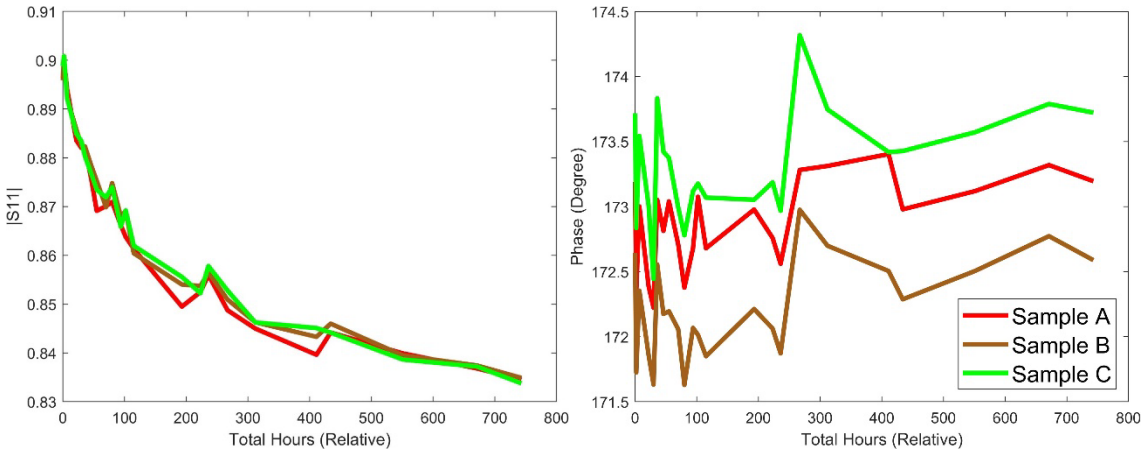

(a) (b)

Figure 3.14: Temporal |S11| (a) and phase (b) of Batch 2, Samples A, B, and C.

Next, the temporal reflection properties of Batch 2, (Na-0 design, ambient, R-Band) at 2 GHz as a function of curing time are shown in Figure 3.14 above. This batch is the same mixture and storage as the S-band samples of Figure 3.13. As was also seen for those samples, |S11| decreases steadily in each sample, with minor variations, reaching a steady state at ~600 hrs (a rate of decrease that is slower that the same measured at S-band).The phase remains effectively constant, with variation remaining within a 1°-to-1.5° range. Next, the temporal reflection properties of Batch 3 (Na-0 design, 60 C, S-Band) are shown in Figure 3.15 at frequency of 3 GHz as a function of curing time.

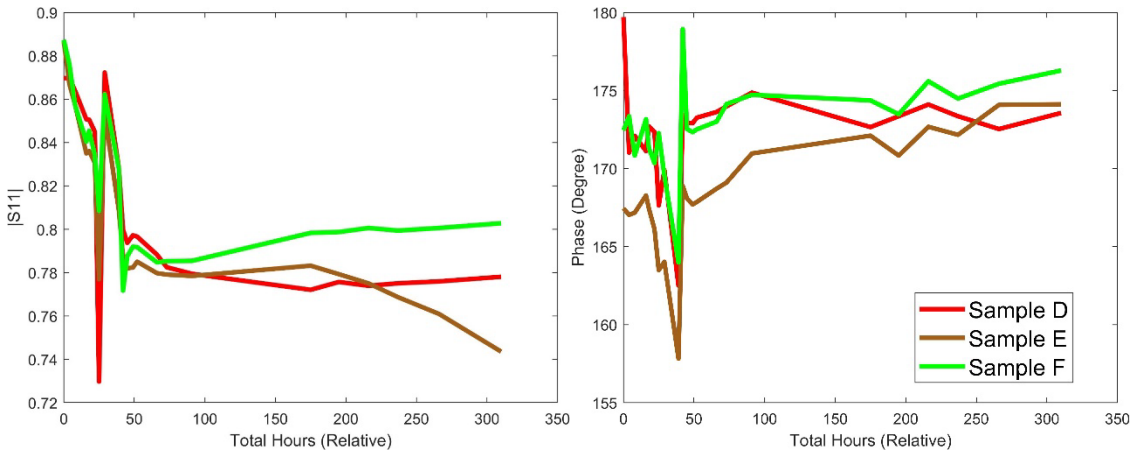

(a) (b)

Figure 3.15: Temporal |S11| (a) and phase (b) of Batch 3, Samples D, E, and F.

Initially, |S11| for all three samples has a negative slope that approaches zero around 50 hours. This indicates that most of the reaction takes place in this time period (much faster than Batch 1, which is an identical sample set except for storage temperature). In addition, there is drastic change at around 25 hours, where a substantial decrease and then increase is evident, with the prior decreasing slope trend reestablished after. These isolated changes are not attributed to chemical changes in the samples, but rather measurement error. The phase of all three exhibits a similar behavior, with more variation (between 10° and 15°) in the first 50 hours, and the slope approaching zero after this time (change within ~5°). Next, the measurement results of Batch 4 (Na-0 geopolymer design stored at 60 C and measured at R-Band) at 2 GHz as a function of curing time are shown in Figure 3.16.

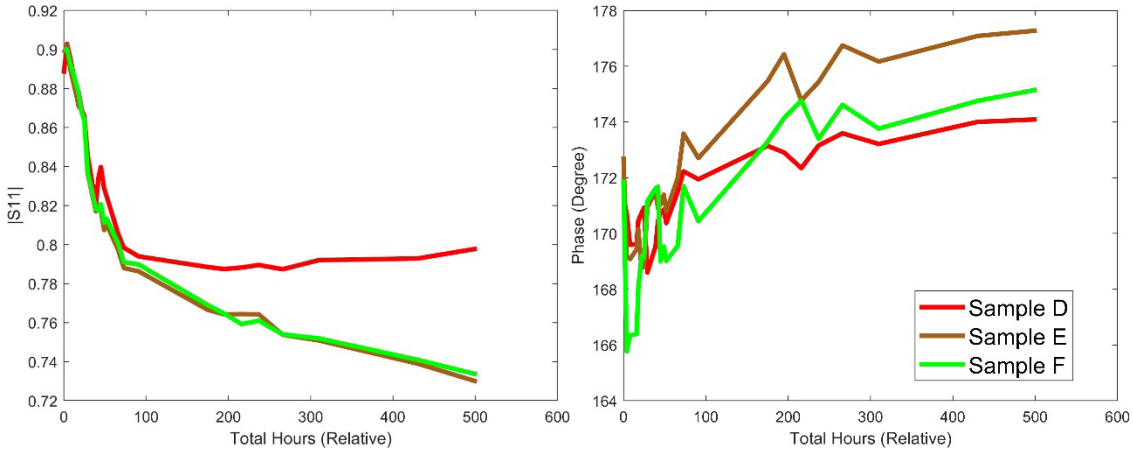

(a) (b)

Figure 3.16: Temporal |S11| (a) and phase (b) of Batch 4 Samples D, E, and F.

As seen in Figure 3.16 above and similar to Batch 3 (Figure 3.15), |S11| decreases (exponentially) in the first 100 hours, before the slope gradually changes to a negative linear slope (E and F, with D approaching zero). In addition, for all three samples, the phase shows measurable and detectable change, with a positive slope over the first 100 hours, with the slope asymptotically approaching 0 after ~100 hours. This is noteworthy since phase for previous batches stays constant as time progresses. The variation in phase occasionally detected throughout the measurement time period is attributed to systematic error and not physical/material changes.

To summarize the notable findings discovered as a result of the reflection measurements on Batches 1-4 (Na-0 mix design with diversity of storage temperature and measurement frequency), The samples in Batches 1 and 2 (cured at ambient temperature) show less change in |S11| than Batches 3 and 4 (cured at 60 C).

Table 3.4 is provided below. As seen in Table 3.4, the maximum average (of all 3 samples) change of |S11| over the measurement period is compared. The samples in Batches 1 and 2 (cured at ambient temperature) show less change in |S11| than Batches 3 and 4 (cured at 60 C).

Table 3.4: Temporal |S11| and phase measurement result comparison for Batches 1-4.

Batch Number	Band	Curing Temp.	Avg |S11| Range	Avg Phase Range (Degree)	|S11| Time to Stabilize (Hr)	Associated Figure
1	S	Ambient	0.06	1	300	Figure 3.13
2	R	Ambient	0.06	2	300	Figure 3.14
3	S	60 C	0.12	3	50	Figure 3.15
4	R	60 C	0.16	6	100	Figure 3.16

This shows a direct relationship between reflection properties (and hence the curing process) and temperature. Similarly, the phase for Batches 3 and 4 (60 C) shows a greater change than the samples cured at ambient temperature. Ultimately, curing temperature has a considerable effect on the temporal measurement results for each sample.

It can also be seen that the effect of frequency manifests in both phase range and |S11| stabilization time. R-Band samples appear to show a greater phase range compared to those measured in S-Band, and |S11| for the samples cured at 60 C stabilizes over a smaller duration of time (e.g., faster curing rate) than that of samples cured in ambient temperature.

3.4.2.2. Na-2 samples. The reflection properties of Batches 5-8 are provided next. These batches used the Na-2 Geopolymer design, which uses a sodium silicate solution. Batches 5 and 6 were measured at S-Band, with Batch 5 cured at ambient temperature and Batch 6 cured at 60 ºC. Batches 7 and 8 were measured at R-Band, with Batch 7 cured at ambient temperature and Batch 8 cured at 60 ºC. First, the reflection properties of Batch 5, (Na-2 design, ambient, S-Band) at 3 GHz as a function of curing time are shown below in Figure 3.17.

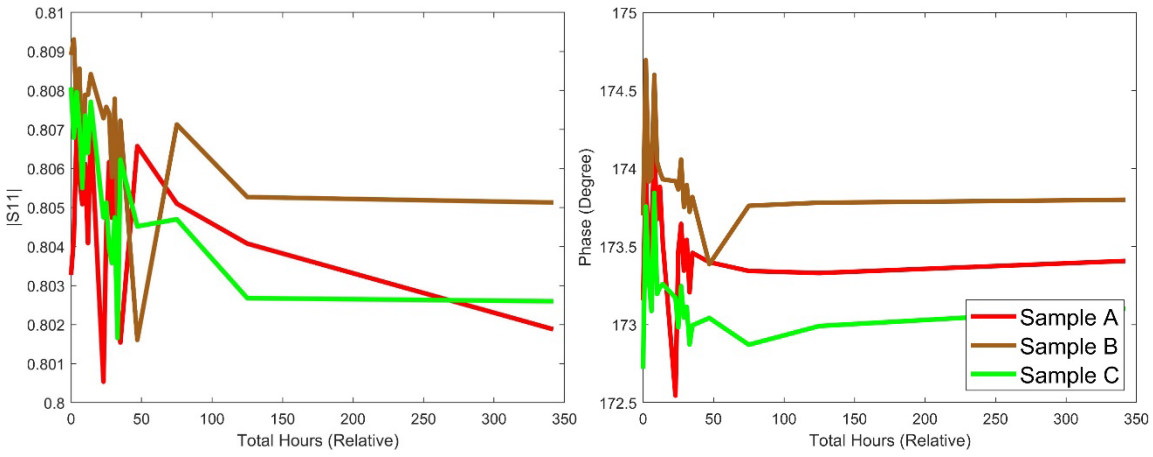

(a) (b)

Figure 3.17: Temporal |S11| (a) and phase (b) of Batch 5 Samples A, B, and C.

As shown above in Figure 3.17, the amount of overall change in |S11| is quite small (~0.8005 to 0.809 as compared to ~0.79 to 0.9 in Batch 4 of Figure 3.16) during the first 50 hours of measurement, followed by a constant (zero slope) response for the remainder of the measurement period. During the first 50 hours, there is evidence of an exponential decrease as seen above, but it is on the order of measurement error and hence overall the response is effectively constant throughout. This indicates that the chemical

changes taking place do not strongly impact the reflection properties of these samples at this frequency band. The same can be said for the phase of the response. In fact, the measurement period is shorter for these samples (as compared to Batches 1-4), reduced as a result of the lack of temporal change in response. Next, the measurement results for Batch 6 (Na-2 design, 60 C, S-Band) at 3 GHz as a function of curing time are shown in Figure 3.18. Here, the measurement result trends of the Batch 6 samples were consistent in |S11| and phase among all three samples and also similar in trend to those of Batches 1-4.

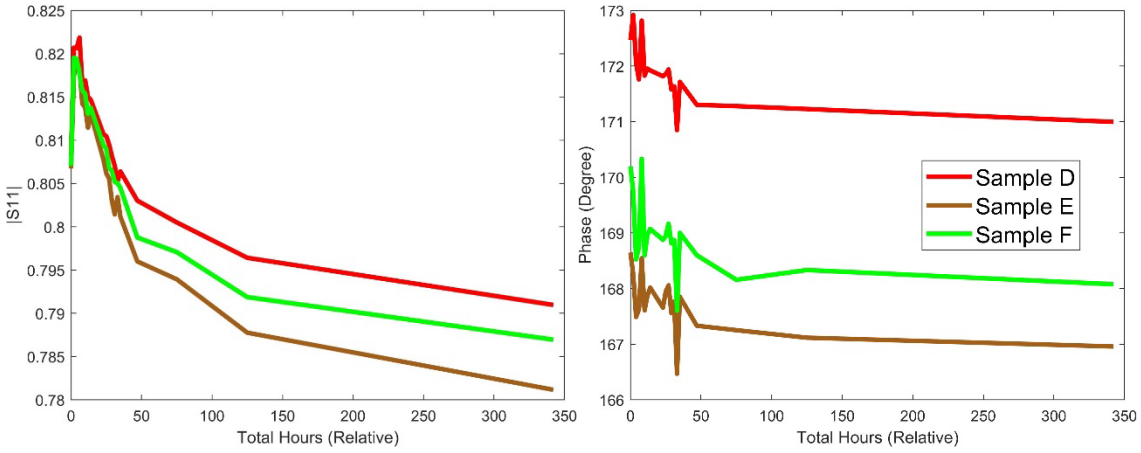

(a) (b)

Figure 3.18: Temporal |S11| (a) and phase (b) of Batch 6 Samples D, E, and F.

More specifically, the occasional measurement error is evident along with a clear exponential decrease in the |S11| through the first 50 hours, with a less substantial but similar outcome for phase. As such and as compared to Figure 3.17, the increase in curing temperature influences the sensitivity of S-band frequencies to the reactions that

take place during the curing cycle. Next, results for the same mix design and temperature, but measured at R-band, are shown in Figure 3.19 and Figure 3.20.

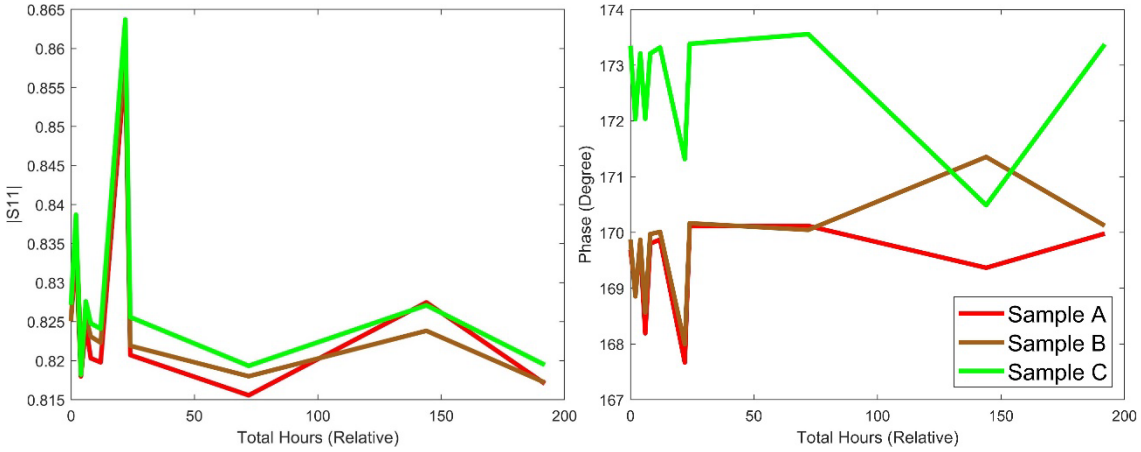

(a) (b)

Figure 3.19: Temporal |S11| (a) and phase (b) of Batch 7 Samples A, B, and C.

As seen for Batch 7, once again the ambient temperature samples exhibit less temporal change, although for R-band, the full range for |S11| is ~0.82-0.86, whereas for S-band, it was ~0.79-0.82. This indicates that frequency (R-Band vs. S-Band samples) may not be sensitive to the chemical reactions that take place during the Na-2 geopolymer curing process. The phase, shown in Figure 3.19b, contains significant measurement error, and any reaction sensitivity is largely obscured as a result. Batch 8, shown below in Figure 3.20, depicts a negative slope with occasional error in the first 25 hours. Similar to other samples stored in 60 C, a reduction of |S11| is evident over the course of the measurement period (0.85 to 0.82). Phase, shown in Figure 3.20b, also shows a limited sensitivity via a slight negative slope.

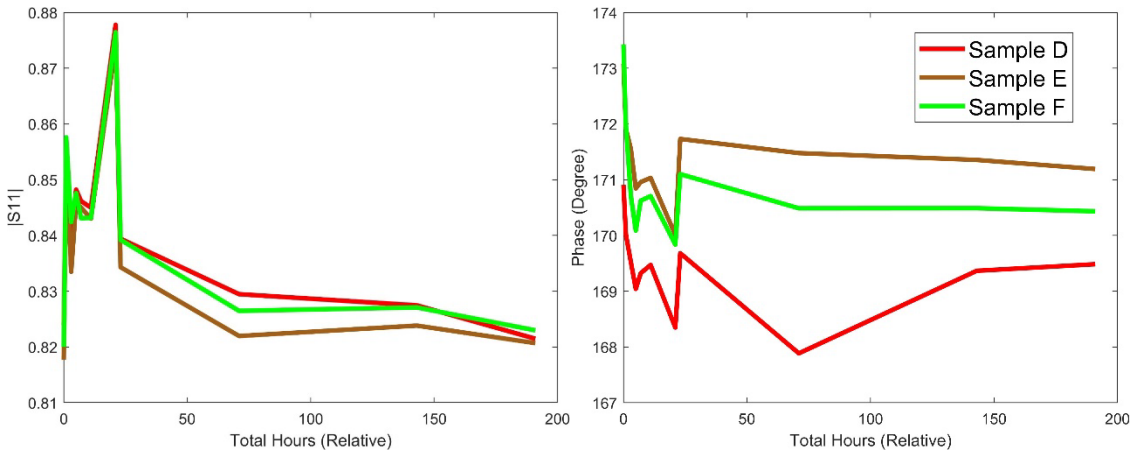

(a) (b)

Figure 3.20: Temporal |S11| (a) and phase (b) of Batch 8 Samples D, E, and F.

In order to draw conclusions on the most significant results from the |S11| and phase measurements from Batches 5-8(Na-2 mix design with varying storage temperature and measurement frequency), Table 3.5 is provided. First, the average change between |S11| for Batches 5-8 is similar amongst all batches and minimal. This indicated that that these frequencies are not sensitive to this particular chemical design. The samples cured at 60 C show more change in |S11| (albeit limited). The phase shows very little change regardless of temperature or band. Stabilization times show R-Band samples reaching stability faster for Batches 5-8. This shows that R-Band measurements may be able to detect faster curing with greater accuracy.

Table 3.5: Temporal |S11| and phase measurement result comparison for Batches 5-8.

Batch Number	Band	Curing Temp.	Avg. |S11| Change	Avg. Phase Change (Degree)	|S11| Time to Stabilize (Hr)	Associated Figure
5	S	Ambient	0.007	2	75	Figure 3.17
6	S	60 C	0.04	2	150	Figure 3.18
7	R	Ambient	0.01	1	25	Figure 3.19
8	R	60 C	0.03	1	75	Figure 3.20

This is consistent with the overall lack of sensitivity evidenced here. To easily compare the effect of frequency specifically, Table 3.6 is provided below. Here a measurement results summary is provided for Batches 1, 3, 5, and 6 (S-Band measurements with diversity in mix design and storage temperature).

Table 3.6: Temporal |S11| and phase measurement result comparison for Batches 1, 3, 5, and 6 (S-Band samples).

Batch Number	Geopolymer Design	Curing Temp.	Avg. |S11| Change	Avg. Phase Change (Degree)	|S11| Time to Stabilize (Hr)	Associated Figure
1	Na-0	Ambient	0.06	1	300	Figure 3.13
3	Na-0	60 C	0.12	3	50	Figure 3.15
5	Na-2	Ambient	0.007	2	75	Figure 3.17
6	Na-2	60 C	0.04	2	150	Figure 3.18

First, more change in |S11| can be seen from the Na-0 Samples. There is no noticeable trend in average change of phase. The time to stabilization appears to be faster on average for Na-2 samples than Na-0 samples, meaning that the reaction in Na-2 designed geopolymer may occur faster than in Na-0 geopolymer. A similar table, but for the R-band samples (Batches 2, 4, 7, and 8) is provided next (Table 3.7).

Table 3.7: Temporal |S11| and phase measurement result comparison for Batches 2, 4, 7, and 8 (R-Band samples).

Batch Number	Geopolymer Design	Curing Temp.	Avg. |S11| Change	Avg. Phase Change (Degree)	|S11| Time to Stabilize (Hr)	Associated Figure
2	Na-0	Ambient	0.06	2	300	Figure 3.14
4	Na-0	60 C	0.16	6	100	Figure 3.16
7	Na-2	Ambient	0.01	1	25	Figure 3.19
8	Na-2	60 C	0.03	1	75	Figure 3.20

First, the Na-0 samples appear to show greater average change in |S11|. Also noticeable is the samples cured at 60 C with geopolymer design Na-0 (Batch 4) shows the most change. This is also seen in Table 3.6 with the average change in |S11| for Batch 3 (cured at 60 C with geopolymer design Na-0) showing the most variation. In addition, Batches 2 and 4 (Na-0 geopolymer design cured at ambient and 60 C respectively) take longer to stabilize than their Na-2 design counterparts.

To conclude, after inspecting a wide range of variables, some trends and relationships are evident. Consistency is observed across all samples showing little

sensitivity from S-Band and R-Band measurements to the particular chemical designs used. Though small, the samples cured at 60 C appear to show more variation in |S11| at S and R-bands. This may reveal that samples cured at 60 C are more sensitive to S-Band and R-Band measurements. Furthermore, the samples of Na-0 design appear to also show slightly more variation in |S11| than those with Na-2 geopolymer design. Across all samples, no discernable trend was noted in phase.

4. MIXING MODELS

4.1. MICROWAVE MATERIALS CHARACTERIZATION

Microwave materials characterization techniques have been shown to be a viable tool for the study of composite mixtures [4]. To this end, they are considered in this work for a temporal characterization of geopolymers [14]. Geopolymers are the product of an alkaline solution mixed with aluminosilicate and in some instances, calcium powder [15]. Geopolymers are emerging as a potential alternative to Ordinary Portland Cement (OPC) concrete and have potential as a reduced-carbon structural material in construction applications [15]. However, as the details on the chemical curing process, in particular the role of (free vs. bound) water, for these materials are not well understood, microwave materials characterization is applied in this work for this purpose [4].

When performing materials characterization on a material that is comprised of multiple components, each individual constituent (and relative volumetric content) contributes to the composite material's effective (or overall) dielectric properties. To this end, if the constituent materials' dielectric properties and volume fractions are known, the effective dielectric properties of the mixture can be calculated via a dielectric mixing model [15]. Mixing models can range from simple (e.g., a linear model with spherical inclusions contained within a host/background material) to more complex (e.g., one that considers other inclusion shapes such as needles or discs).

As it relates to this work, the effective dielectric properties of geopolymer samples will be determined using a linear mixing model and the measured constituent dielectric properties (and respective volume fractions), with the overall goal of studying

the temporal role of free vs. bound water during the curing process. Specifically, the constituents consist of the geopolymer precursor powder, or GPP, air (void content/porosity), which occupies the space between the powder particulate (and is considered as part of the effective material when the powder is measured), along with the alkaline solution and (free) deionized (DI) water. In this case, the GPP considered is metakaolin.

4.2. GEOPOLYMER CONSTITUENTS

Two alkaline solutions were chosen in order to mix two different geopolymer designs, namely, a sodium hydroxide solution, referred to as Na-0, and a sodium silicate solution, referred to as Na-2. When mixed with metakaolin powder and DI water, these components form the geopolymer. Prior to mixing, the dielectric properties of each constituent material were measured using a two-port rectangular waveguide measurement [11], and/or one-port open ended waveguide measurement [16], depending on material properties, amount of material available for measurement, etc. The measured values for each constituent can be found in Table 4.1 below, along with the bands in which they were measured. These frequency bands were chosen based on desired frequency ranges that have shown sensitivity to free and bound water, namely, S (2.6-3.96 GHz)- and R (1.72-2.6 GHz) bands [4], along with measurement limitations related to available materials and chemical concerns related to contact with conductive materials.

In addition to constituents, Table 4.1 also contains the dielectric properties of two resultant materials that are created after mixing and as the geopolymer cures. The first is referred to as pore solution, which is a liquid that forms within the pores of the

geopolymer as it cures. For this work, the pore solution is assumed to be free (DI) water. The next, geopolymer paste, is the chemical combination of the constituents as they bond into a geopolymer. For characterization purposes, a mixing model will be used to approximate its dielectric properties from the constituent materials (Metakaolin Powder, DI Water, and Alkaline solution, both Na-0 and Na-2). Note that G-band (3.95-5.85 GHz) and R-band were used to measure the constituents (Metakaolin Powder, DI Water, Na-0 and Na-2 solutions) used for the mixing model used to approximate the dielectric properties.

Table 4.1: Dielectric Properties of Geopolymer Material

Material	ε_r	**Frequency Band**
Metakaolin Powder	1.79 - *j*0.02	R
DI Water	77 - *j*0	G
Na-0 Solution	4.82 - *j*0.03	G
Na-2 Solution	12.20 - *j*1.85	G
Unreacted Metakaolin	1.79 – j0.02	R
Free Water (Pore Solution)	77 - j0	R
Paste (Geopolymer Gel)	Unknown	-

4.3. DIELECTRIC MIXING MODEL

Using the measured dielectric properties of each constituent and the respective volume fraction of each, a dielectric mixing model can be used to determine the effective

dielectric properties of a composite material (in this case, the geopolymer). The power law mixing model [19] is used in order to determine the effective dielectric properties, ${\varepsilon_{Eff}}^n$, where *n* is the order and for this work is equal to 0.5:

$${\varepsilon_{Eff}}^n = (\varepsilon_1)^n\, Vf_1 + (\varepsilon_2)^n\, Vf_2 + (\varepsilon_3)^n\, Vf_3 + \cdots + (\varepsilon_x)^n\, Vf_x \quad (1)$$

For geopolymer paste, ε_1, ε_2, and ε_3 are equal to the respective ε_r for Metakaolin, DI Water, and Alkaline solution (Na-0 or Na-2 depending on the mixture design), all shown above in Table 4.1. Vf_1, Vf_2, and Vf_3 are the volume fractions of each constituent, Metakaolin, DI Water, and Alkaline solution, respectively. For the effective geopolymer mixture, ε_1, ε_2, and ε_3 are equal to the respective $\boldsymbol{\varepsilon_r}$ for unreacted metakaolin, pore solution, and paste, respectively. Vf_1, Vf_2, and Vf_3 are equal to the volume fraction for each unreacted metakaolin, pore solution, and paste, respectively. These values were provided by collaborators and can be found below in Table 4.2 and Table 4.3 (and illustrated temporally in Figures 4.1 and 4.2). As seen in Figure 4.1and Figure 4.2, the volume fractions of the pore solution, paste, and unreacted metakaolin change temporally over the course of the measurement period, with a majority of the change taking place in the first 25 hours. In all cases, the volume fraction of geopolymer paste increases over the course of the measurement period, with the volume fraction of unreacted metakaolin decreasing, and the volume fraction of pore solution changing very little. By using the power law model from Equation 1, the dielectric properties of the geopolymer paste can be calculated from the volume fractions and dielectric properties of the constituents. The calculated dielectric properties for the effective geopolymers (both designs and both curing temperatures) are shown below in Table 4.4.

Table 4.2: Constituent and resultant material volume fractions over measurement period, per Na-0 design and curing temperature.

		Volume Fraction Over the Measurement Period						
Design	**Material**	**Starting Mix**	**3 Hr**	**6 Hr**	**12 Hr**	**24 Hr**	**78 Hr**	**196Hr**
Na-0	Na-0	14.87	-	-	-	-	-	-
	DI-Water	58.93	-	-	-	-	-	-
	Metakolin	26.20	-	-	-	-	-	-
	Pore Solution	0	21.18	21.88	25.31	27.69	26.33	26.24
	Paste	0	53.33	53.79	52.77	53.11	58.85	61.92
	Unreacted Metakaolin	0	25.48	24.34	21.91	19.20	14.81	11.84
Na-2	Na-2	16.97	-	-	-	-	-	-
	DI-Water	57.48	-	-	-	-	-	-
	Metakaolin	25.55	-	-	-	-	-	-
	Pore Solution	0	27.68	30.24	33.81	35.29	32.94	33.86
	Paste	0	42.95	41.83	43.86	45.41	51.19	54.50
	Unreacted Metakaolin	0	29.37	27.93	22.33	19.31	15.87	11.65

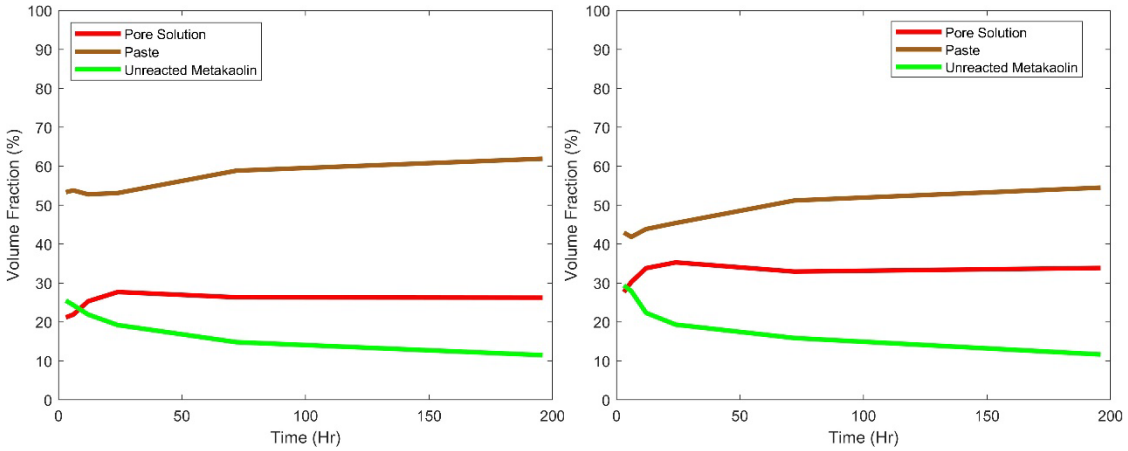

(a) (b)

Figure 4.1: Geopolymer constituent composition at 23° C (a) Na-0 and (b) Na-2.

Table 4.3: Constituent and resultant material volume fractions over measurement period, per Na-2 design and curing temperature.

		Volume Fraction Over the Measurement Period						
Design	**Material**	**Starting Mix**	**3 Hr**	**6 Hr**	**12 Hr**	**24 Hr**	**78 Hr**	**196 Hr**
Na-0	Na-0	14.87	-	-	-	-	-	-
	DI-Water	58.93	-	-	-	-	-	-
	Metakaolin	26.20	-	-	-	-	-	-
	Pore Solution	0	26.35	30.51	19.22	21.77%	21.18	21.41
	Paste	0	50.63	48.07	60.89	59.88%	66.07	65.70
	Unreacted Metakaolin	0	23.03	21.42	19.89	18.35%	12.75	12.89
Na-2	Na-2	16.97	-	-	-	-	-	-
	DI-Water	57.48	-	-	-	-	-	-
	Metakaolin	25.55	-	-	-	-	-	-
	Pore Solution	0	32.69	41.28	48.16	32.19%	31.24	30.90
	Paste	0	39.35	34.40	30.33	47.58%	53.46	56.49
	Unreacted Metakaolin	0	27.96	24.33	21.51	20.22%	15.30	12.61

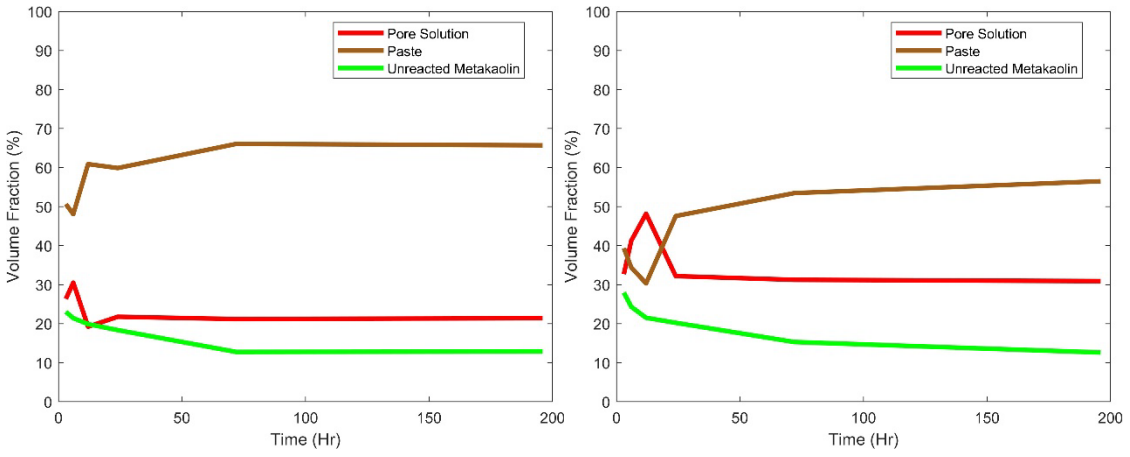

(a) (b)

Figure 4.2: Geopolymer constituent composition at 60° C (a) Na-0 and (b) Na-2.

Table 4.4: Calculated effective dielectric properties for geopolymers over the measurement period.

	Na-0 Design		Na-2 Design	
Time (Hours)	23°	60°	23°	60°
3	28.28 - j0.04	31.15 - j0.04	29.34 - j0.22	31.59 - j0.21j
6	29.07 - j0.04	33.35 - j0.04	30.86 - j0.22	36.32 - j0.20j
12	31.36 - j0.04	30.4 - j0.04	35 - j0.24	40.28 - j0.18j
24	33.55 - j0.04	32.01 - j0.04	37.2 - j0.25	35.64 - j0.26j
72	35.4 – j0.04	34.73 - j0.04	38.39 - j0.28	38.15 - j0.29j
196	36.93 - j0.04	34.73 - j0.04	41.22 - j0.3	39.61 - j0.31j

4.4. SIMULATION

Using the calculated effective permittivity and loss factor of the geopolymer (shown in Table 4.4 above), full wave high frequency simulations can be conducted in order to determine if the calculated temporal effective dielectric properties properly represent the samples. These simulations, conducted using CST Microwave Studio™, assume a material with the properties shown in Table 4.3 is placed within a SC-RWG sample holder.

Such a sample holder is illustrated in Figure 4.3 and a simulation at S-band was performed in order to analyze the complex reflection properties, S11. The S-band

samples were selected to illustrate the process, as the R-band samples provided similar measured results. These results were compared with sample measurements as described in Section 3, where a sample length of 37 mm was chosen along with a 37 mm long sample holder (commensurate with the physical samples and sample holders).

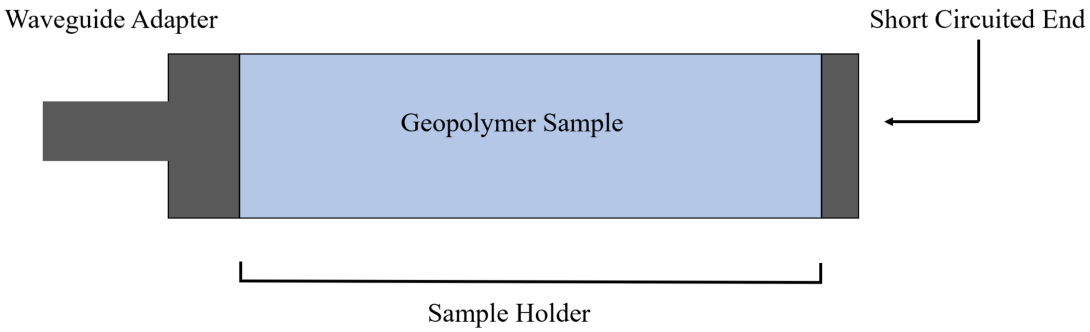

Figure 4.3: Simulated Short Circuit Waveguide Model

Below, the results for |S11| and phase for each simulation can be found in Figures 4.4 through 4.7, compared with measurements (from Section 3). As shown below in Figure 4.4 (Na-0 Samples cured at 23 °C), the simulated |S11| varies repetitively across the band between 0 and -1 dB throughout the measurement time period of interest.

Comparatively speaking, the measured |S11| varies linearly over the range of -1 to -2 dB and decreases with increasing frequency. This decrease as a function of frequency is not evident in the simulated |S11|. Furthermore, the simulation exhibits several resonances across the frequency band, none of which are evident in the measurement. This indicates an inaccurate representation of the dielectric properties and/or volume fraction of the samples that were used for simulation.

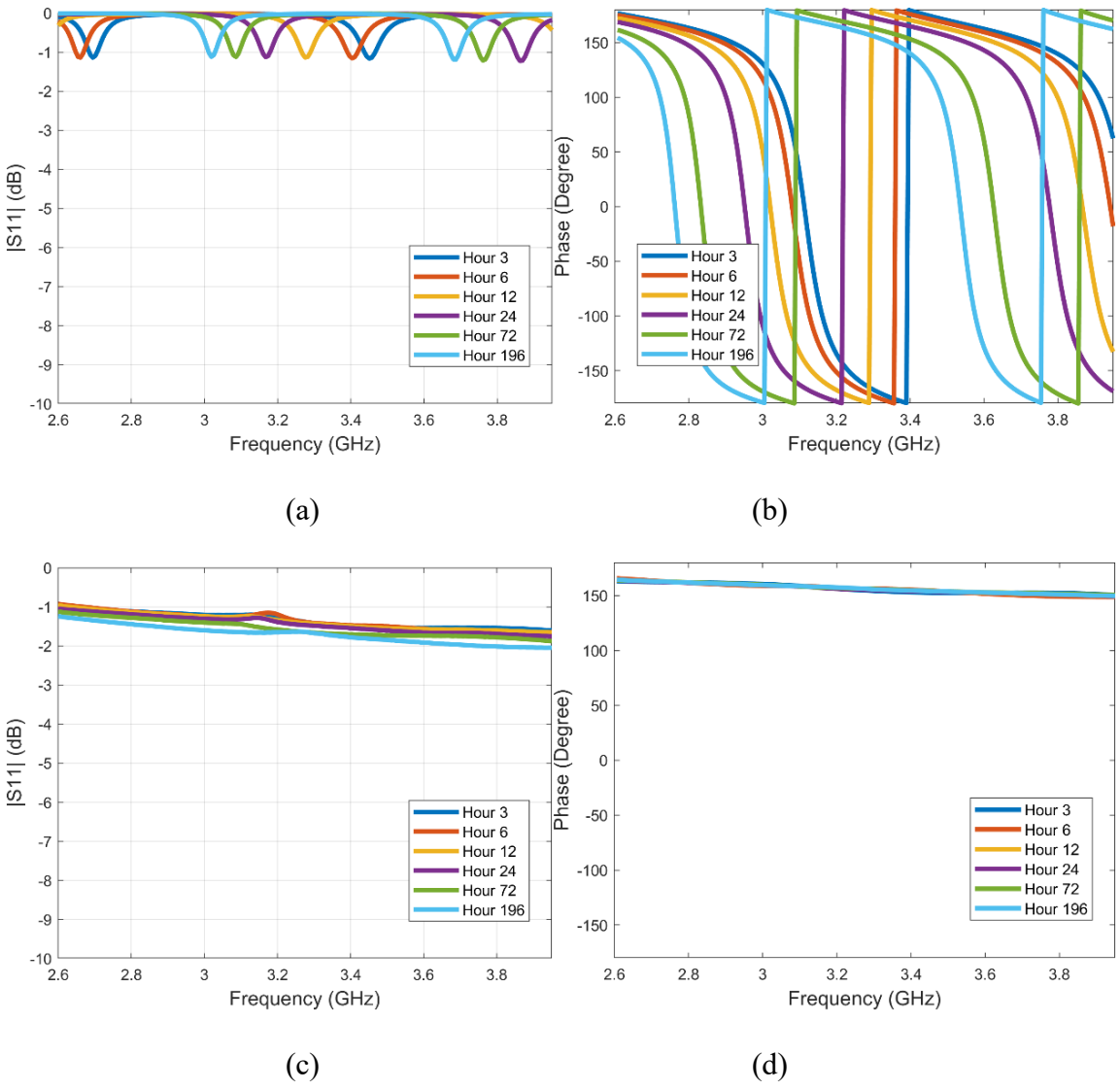

Figure 4.4: Simulated (a) and (b) and measured (c) and (d) |S11| and phase (respectively) of Na-0 geopolymers cured at 23°C over the measurement period.

However, as many assumptions have been made (as noted above) including the composition of the pore solution and the dielectric properties of the paste over the curing period, it is not reasonable to expect precise agreement. Rather, agreement in trends is of more importance. In this case and ignoring the resonances, the |S11| for simulation and measurement are on the same order of magnitude (a few dB). The simulated and

measured phase do not agree, as the measured phase is within the range of ~180º - 170º, and the simulated phase is ~+/- 180°. However, with assumptions made, this is not unexpected.

As shown in Figure 4.5 (simulated and measured results for Na-0 geopolymer cured at 60 °C) below, the simulated |S11| varies between 0 and -1 dB, with resonances apparent throughout the frequency range.

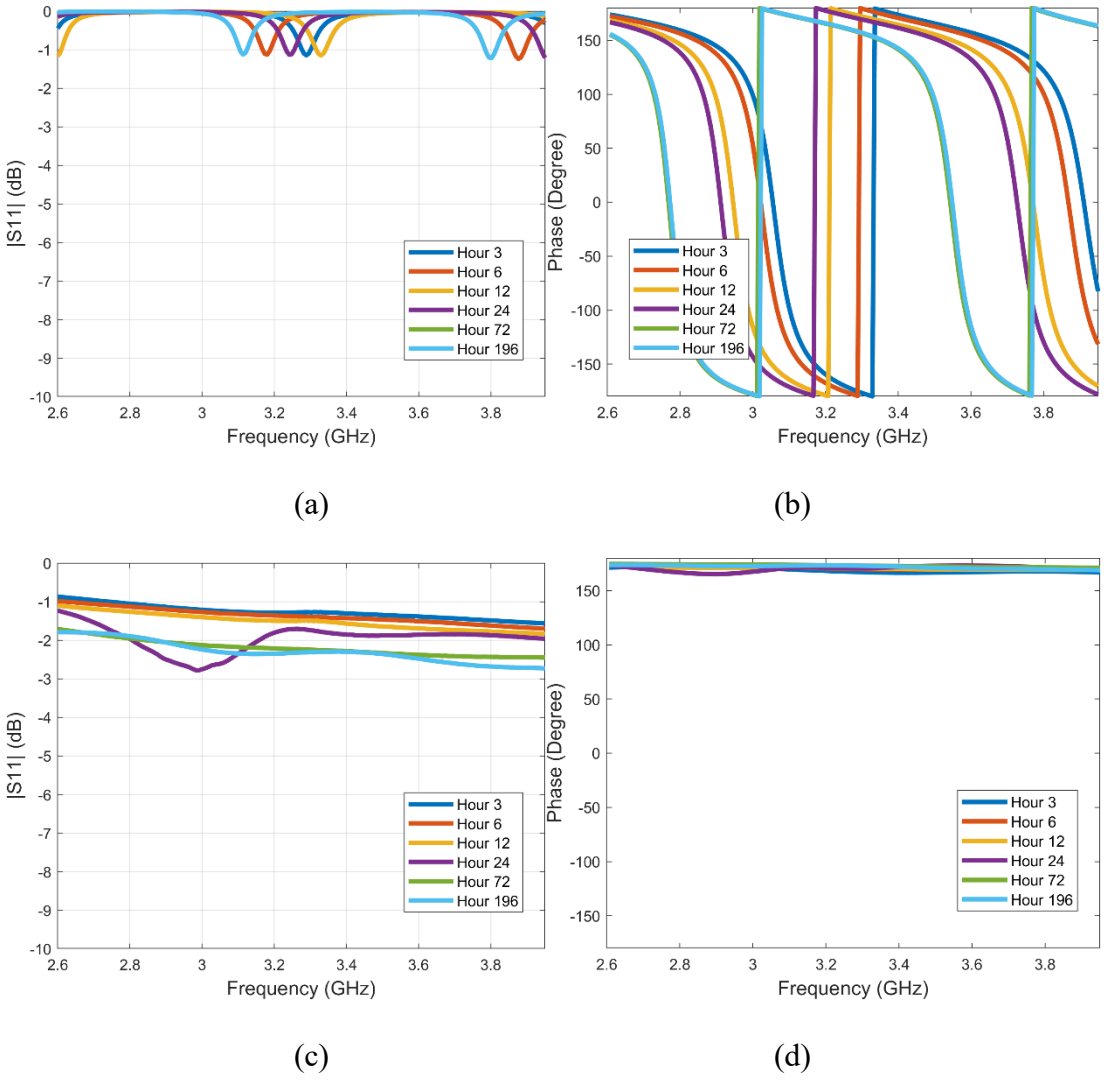

Figure 4.5: Simulated (a) and (b) and measured (c) and (d) |S11| and phase (respectively) of Na-0 geopolymers, cured at 60°c, over the measurement period.

The measured |S11| ranges from -1 to -3 dB and decreases linearly as frequency increases. Comparing the simulated and measured |S11|, trends between the two are apparent. That is to say, the simulated |S11| and measured |S11| are within a few dB of each other, and both do not show variance greater of 2 dB. The simulated Phase varies from -180° to 180° as frequency increases, whereas the measured phase is near 175° regardless of the frequency.

Again, as many assumptions regarding the characterization of the constituent materials were made, precise agreement is not expected. Lastly. |S11| and Phase also behave similarly to the Na-0 samples measured at 23 ºC, shown in Figure 4.4.

Provided below, Figure 4.6 shows the simulated and measured results for the Na-2 geopolymer design cured at 60 °C. First, |S11| of the simulated samples shows resonances of less than -10 dB over the frequency band. Phase varies between +/- 180°. |S11| of the measured results ranges from -1 to -3 dB, with phase remaining constant at ~170°. For the measured results, |S11| decreases linearly with frequency, and phase remains constant across the band, similar to that of the previous measurements shown in Figure 4.4 and Figure 4.5. Also as above, these results show that while the simulated parameters are still affected by the assumptions regarding the constituent materials characterization to accurately portray the geopolymer, trends between simulation and measurement remain.

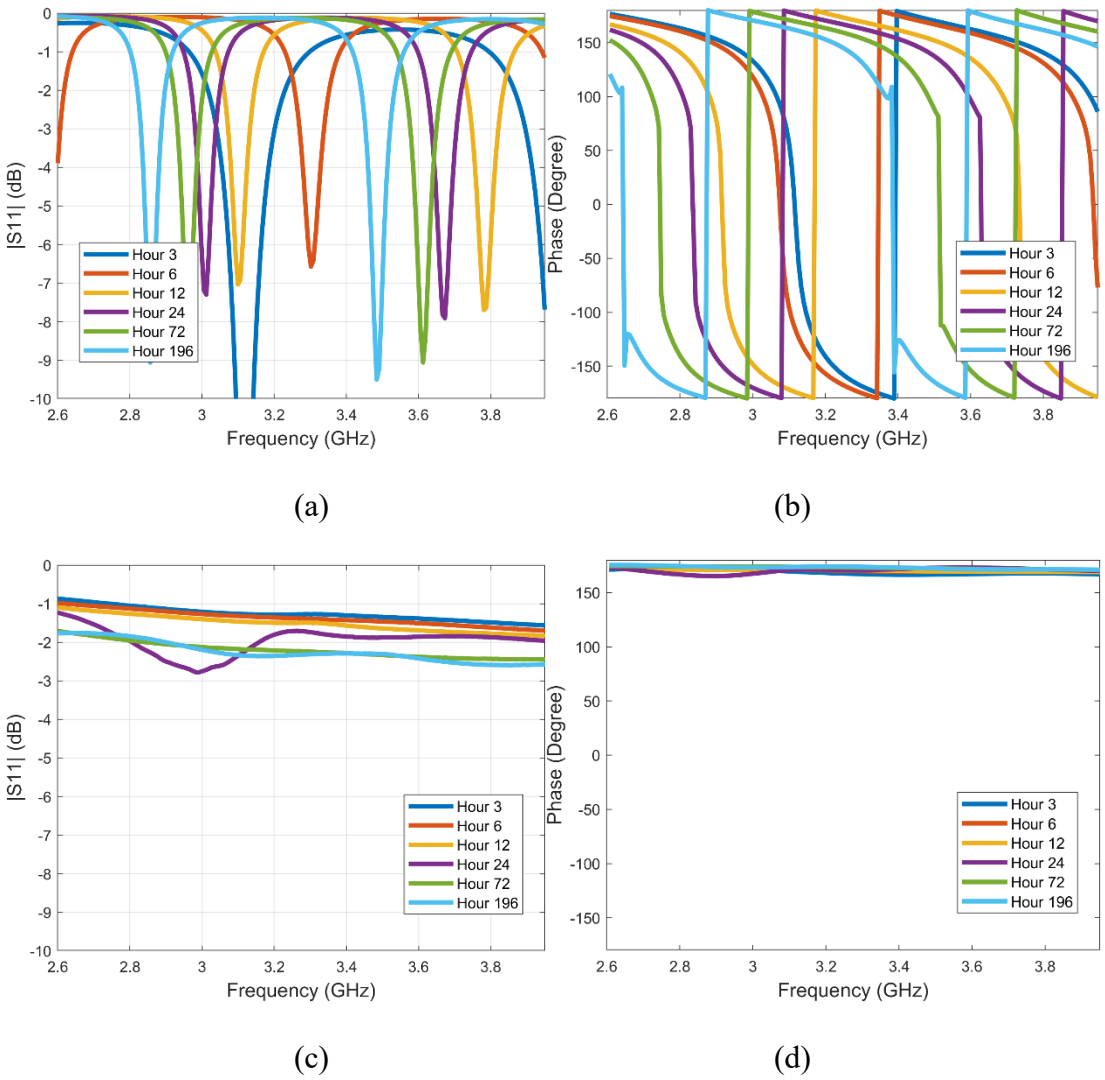

Figure 4.6: Simulated (a) and (b) and measured (c) and (d) |S11| and phase (respectively) of Na-2 geopolymer samples, cured at 23°C, over the measurement period.

Lastly, Figure 4.7 below shows the simulated and measured results of the Na-2 geopolymers cured at 60 °C. Similar to the simulation results shown in Figure 4.6, |S11| of the simulated geopolymer exhibits resonances of the same magnitude (on the order of 10 dB). Also, similar to all previous simulations, the phase varies between +/- 180°. The measured |S11| once again decreases linearly from -1 dB to -3 dB with phase remaining

constant at 170. Trends between simulation and measurement persist overall, as seen in the other data sets.

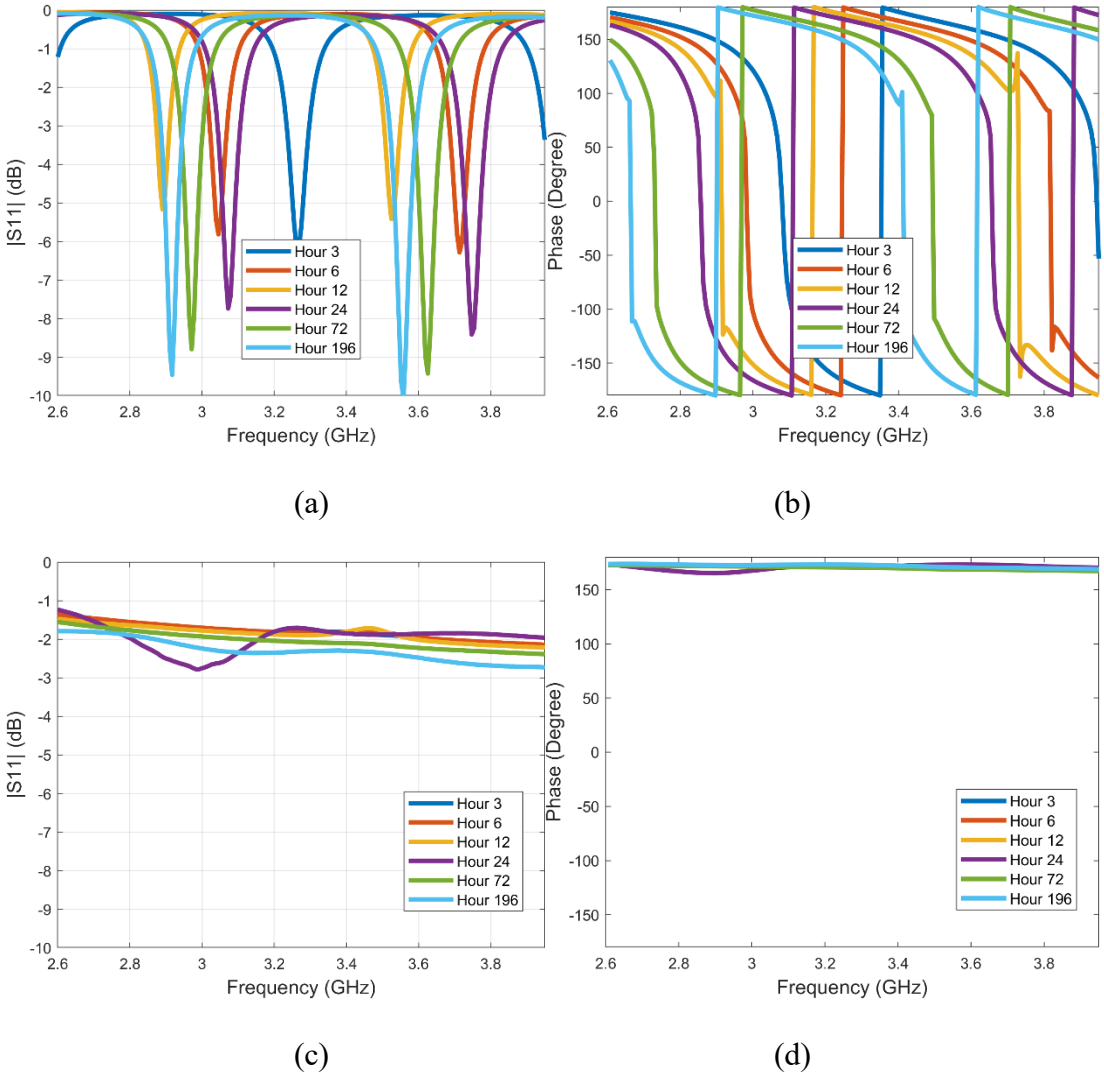

Figure 4.7: Simulated (a) and (b) and measured (c) and (d) |S11| and phase (respectively) of Na-2 geopolymer sample, cured at 60°C, over the measurement period.

As shown above, the process for a forward iterative model that can be used to iteratively determine dielectric properties of composite materials such as a geopolymer has been established. However, the inputs available at this time are not sufficient to

determine information about the constituents with certainty, as evidenced by the differences in measured and simulated results. In other words, while general trends are evident, precise agreement remains to be achieved.

To this end, in order to illustrate the application of the iterative process in such a way as to obtain improved agreement, the Na-0 sample cured at 23 °C is considered, shown in Figure 4.4c and d. As stated, the volume fractions of the constituents have been physically quantified and therefore are considered known constants. The same can be said for the measured dielectric properties of metakaolin, alkaline solutions, and DI water. However, unknowns that remain are the dielectric properties of the geopolymer paste and pore solution, along with additional (unexpected and unknown) chemical reactions.

Recall that the current study assumes the dielectric properties of pore solution are equal to that of DI water and the dielectric properties of geopolymer paste are equal to the combined (and calculated) dielectric properties of DI water, metakaolin, and alkaline solution. To this end, the dielectric properties of the overall material have been iteratively revised such that the agreement between simulation and measurement is improved. Figure 4.8 below shows the simulation results of a sample of $\varepsilon_r = 1 - j7$ for sample lengths of 37 mm (the actual sample length) and 5 mm (for comparison). A representative measurement of the 37 mm Na-0 sample, measured after curing at 23 °C for 24 hours is also provided.

As can be seen in Figure 4.8 below, the simulated reflection properties for the 37 mm long sample does not agree with the measured sample of the same length, showing a reduction in magnitude of ~2 dB, while the phase spans from 150° to 125° (much closer

to the measurement result of ~170° to 150°). The results for the 5 mm long sample, however, approximates the measured geopolymer much closer in magnitude, with a similar result in phase. In this case, the simulated magnitude ranges from ~-0.5 dB to -2 dB, whereas the measurement ranges ~-1 dB to -2 dB.

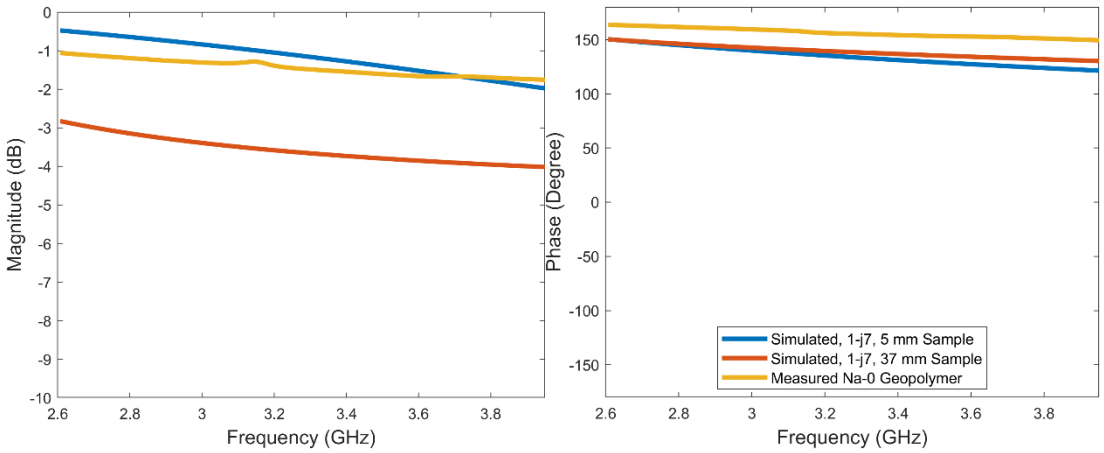

(a) (b)

Figure 4.8: Measured Na-0 geopolymer, (cured for 24 Hours at 23 °C) and simulated Na-0 geopolymer of $\varepsilon_r = 1 - j7$ with a length of 37 mm And 5 mm: magnitude (a) and phase (b).

Overall, the behavior of both magnitude and phase from the simulated 5 mm sample agree with the measured geopolymer much more than the simulated geopolymer using the outputs of the mixing model shown in Figure 4.4a and b, and the 37 mm long simulated geopolymer shown in Figure 4.8. Of course, the value of dielectric properties and sample length do not represent the physical specimens, as a relative permittivity of 1 represents free space (air), and the SC-RWG was not empty. However, it is possible that there was a small gap between the measurement end of the SC-RWG sample holder that occurred at the sample cured due to shrinkage. In addition, the value of phase for the

measured samples (on the order of 170° to 150°) is representative of a fully reflective load (which provides a reflection coefficient of -1, or a phase of +/-180°). Therefore, it is postulated that, due to the actual dielectric properties of the geopolymer sample, a "half wave transformer" scenario has resulted, meaning that the impedance of the SC-end is reflected to the measurement port (or near it, accounting for the air gap) and therefore the measured reflection properties will be similar to those of a SC (0 dB with a phase of 180°) [13]. It should be noted that the magnitude of (all) measurements was less than 0 dB, meaning there is some signal interaction with the samples, but the overarching measured result may be dictated by the SC-termination, rather than the samples themselves. Future refinement for measurement of this type of material would include shorter sample lengths to avoid the "half wave transformer" phenomenon. More information on the dielectric properties of the unknown pore solution and paste would also significantly improve the application of the model developed in this work to the measured results.

Overall, the simulated geopolymer sample results obtained using the dielectric properties calculated via the mixing model do not accurately match the measured results. The simulated samples showed greater variance in |S11| across the band, often with significant resonances. Additionally, the range of |S11| was greater. Phase consistently exhibited a different response between simulation and measured as well. Despite these differences, a mixing model can be a useful tool to roughly predict material behavior with little difficulty, as a simple equation can be used that allows the user to create a

generalization of expected reflection behavior. These models can be used as an initial guess for calculating dielectric properties iteratively or could be used to understand what behavior a mixture may have before it is created.

5. SUMMARY AND FUTURE WORK

5.1. BACKGROUND

Geopolymers are a promising potential alternative to OPC concrete for civil and commercial applications [1]. A chemical reaction between an activating powder, an alkaline solution, and water are used to create these structural binders [1]. The chemical reactions that take place during the curing process, including the role of water and its binding state (free vs. bound) during the curing process, is not fully understood. To this end, as microwaves have been shown to be sensitive to the free and bound states of water, microwave materials characterization is one such option to study the curing process and the role and state of water during the same. As such, a simulation and measurement-based study was undertaken to better understand these materials as they cure.

The measurements aspect of this study was completed on the geopolymer samples, throughout the curing cycle, as the material changes from a liquid to solid state. As such, a sample holder was needed that would facilitate measurement of both states of the material while keeping the (free) water within the sample (i.e., minimizing evaporation). Therefore, a short-circuited rectangular waveguide (SC-RWG) sample holder was designed to hold the geopolymer materials.

The simulation aspect of this study featured a full wave model that determined reflection properties of a given material placed within a short-circuited rectangular waveguide sample holder. This model utilized calculated dielectric properties for the material within the SC-RWG that were determined via a dielectric mixing model. This mixing model considered measured dielectric properties of the geopolymer constituents

and volumetric fraction information provided by collaborators to calculate overall (effective) dielectric properties. Simulated reflection properties were then compared to measurements of two different geopolymer designs cured at two different temperatures. The degree of agreement between simulated and measured results provides insight into the geopolymer curing reactions as well as the assumptions made within the modeling process.

5.2. SHORT CIRCUIT RECTANGULAR WAVEGUIDE APPROACH

As mentioned, a short-circuited rectangular waveguide (SC-RWG) was chosen for the geopolymer sample holder due to the liquid-to-solid state of the material. In order to successfully use the SC-RWG for this approach, the effect of a sample's placement, length, and dielectric properties on the measurement must be fully understood. Previously as reported in the literature, it was understood that sample placement was critical for SC-RWG materials characterization measurements, due to the importance of placing the sample at a maximum of the electric field in order for the sample to adequately interact with the electric field in the waveguide. This study found that samples of length greater than $\lambda_g/6$ interact with the electric field in such a way as to produce meaningful materials characterization measurements, regardless of the dielectric properties of the sample. Although samples of low permittivity and loss factor that have length of less than $\lambda_g/6$ must be placed at a maxima, usually $\lambda_g/4$, it was found that high permittivity and loss factor samples of lengths less than $\lambda_g/6$ may be placed at the short-circuit end of the waveguide. As the material of interest is in liquid form at casting, this outcome was critical for the experimental portion of this work. In other words, the findings in this

section indicated that the mixture may be poured into the sealed sample holder, rather than be shifted (by way of an additional material in the SC-RWG) to an electric field maximum.

5.3. GEOPOLYMER MEASUREMENT CONSIDERATIONS

Over a 200 hour measurement period, the SC-RWG measurement approach was utilized to measure complex reflection properties of geopolymer samples of two mix designs, referred to as Na-0 and Na-2, and two curing temperatures, 23 C and 60 C, in two bands, R-Band and S-Band. The results show that the reflection properties undergo the most change in the first 50 hours of the curing process for both bands and mix designs. The samples cured at 60 C show more variation in |S11| at both bands, which could suggest that both S- and R-band are equally sensitive to the curing process of these geopolymers at this temperature. The complex reflection properties of the Na-0 design showed slightly more variation in |S11|, also indicating equal sensitivity at both bands (over the Na-2 design).

5.4. MIXING MODELS

A power law mixing model was applied to estimate the effective dielectric properties of the geopolymers using the properties and volume fractions of the constituents (metakaolin powder, alkaline solution, and DI water). It was assumed that the dielectric properties of geopolymer paste are equal to that of the mixture of metakaolin powder, alkaline solution, and DI water, and that the dielectric properties of pore solution are equal to those of DI water. Using the outcome of the mixing model, full

wave simulations were performed in order to calculate the reflection properties (magnitude and phase) from such a material when placed in a SC-RWG sample holder of length identical to those of measurement. The simulated results were compared to measured results. Although the simulated and measured results did not agree resulting from (at least in part) assumptions regarding the composition of the samples and application of the mixing model, there was agreement in the general trend of measured vs. simulated results. The simulations suggest that the high permittivity of DI water present in the assumed values for paste and pore solution may have affected the accuracy, as does the potential for unaccounted-for air in the samples (porosity).

To further investigate the impact of the assumptions and determine representative dielectric properties of the samples that provide a simulation that is reasonably similar to measurement, simulations of samples with lengths of 37 mm (actual sample length) and 5 mm (much smaller and on the order of the estimated air gap that was present in the samples) were conducted. The relative dielectric properties used in these additional samples are 1 - j7. The results for the 5 mm sample length compared fairly well to the measured 37 mm sample (a fairly reflective response with a phase similar to that of a SC). However, these dielectric properties do not represent a physically realistic material (1 represents an empty waveguide with no dielectric polarization/energy storage whereas -j7 represents a significantly lossy/absorptive material). Therefore, it is theorized that the geopolymer's actual dielectric properties may have created a "half-wave transformer," reflecting the impedance of the short circuit close to the measurement port. The dieletric properties of the pore solution and paste are also important, and future work to better

understand those materials would also be invaluable as it relates to the refinement of this modeling effort.

While the measurements and measurement techniques performed in this work proved effective at providing a method for reflection measurement of liquid-to-solid samples while minimizing evaporation, there are a number of aspects that can be refined to improve the agreement between the modeling and measurements. This includes:

- The inclusion of an iterative routine for calculating S-Parameters from SC-RWG measurements. This would allow for a direct calculation of the effective dielectric properties of the samples over time which would in turn provide insight about unknowns within the curing process.
- More measurements can be taken across different frequency bands in order to better understand each material. While consistency among geopolymer designs was shown in the observed the S- and R-bands, other bands may be more sensitive to the chemical processes and curing mechanisms specific to these particular geopolymer designs.
- Additional simplified sample mix designs can be considered to provide insight on important fundamental materials like paste and pore solution. Without further information on these aspects of more complex geopolymer mixtures, it is very challenging to study the more complex materials. A better understanding of the fundamental inputs of geopolymers will also aid in determining sample lengths, etc. (with the goal of avoiding a half-wave transformer case, which can be detrimental for materials characterization purposes).

- Now that a better idea of the dielectric properties of geopolymer materials is available, the sample lengths can be revisited to ensure that the “half wave transformer” scenario is avoided.
- Further work can be done to evaluate the roll of water in the geopolymer curing process, as water is closely linked to pore solution, and geopolymer paste.

BIBLIOGRAPHY

[1] Alkali activated materials: State-of-the-art report, Rilem TC 224-AAM, ed. J.L. Provis and J.S.J. van Deventer. 2014: Springer/RILEM.

[2] Duxson, P., Provis, J.L., Lukey, G.C. and van Deventer, J.S.J., The role of inorganic polymer technology in the development of 'green concrete', Cement and Concrete Research, 2007. 37 (12): pp. 1590-1597.

[3] C. A. Edwards, K. M. Donnell and C. R. Shearer, "Microwave materials characterization of geopolymer precursor powders," *2018 IEEE International Instrumentation and Measurement Technology Conference (I2MTC)*, Houston, TX, USA, 2018, pp. 1-5, doi: 10.1109/I2MTC.2018.8409709.

[4] A. Hashemi., M. Horst, K. E. Kurtis, K. M. Donnell, and R. Zoughi, "Comparison of alkali–silica reaction gel behavior in mortar at microwave frequencies," *IEEE Trans. on Instrumentation and Measurement*, vol. 64, no 7, pp. 1907-1915, 2015.

[5] A. H. Sihvola, *Electromagnetic Mixing Formulas and Applications*. Institution of Electrical Engineers, 1999.

[6] J. Sinkey, A. Hook and K. M. Donnell, "Sample Considerations for Short-Circuited Filled Transmission Line Measurements," *2023 IEEE International Instrumentation and Measurement Technology Conference (I2MTC)*, Kuala Lumpur, Malaysia, 2023, pp. 1-6, doi: 10.1109/I2MTC53148.2023.10175977.

[7] R. Zoughi, S. D. Gray, and P. S. Nowak, "Microwave nondestructive estimation of cement paste compressive strength," *ACI Materials Journal*, vol. 92, no. 1, 1995.

[8] S. Peer, T. Case, K. Donnell, D. Hughes, R. Zoughi, and K. Kurtis. "Investigation of microwave reflection properties of mortar exposed to wet-dry cycles of tap water and chloride bath," *Quantitative Nondestructive Evaluation*, vol. 615, no. 1, pp. 1269-1276, 2002.

[9] X. Lin and B. -C. Seet, "Dielectric Characterization at Millimeter Waves With Hybrid Microstrip-Line Method," in *IEEE Transactions on Instrumentation and Measurement,* vol. 66, no. 11, pp. 3100-3102, Nov. 2017, doi: 10.1109/TIM.2017.2746362.

[10] S. Julrat and S. Trabelsi, "Free-Space Transmission Dielectric Properties Measurement Based on Six-Port Technology," in *IEEE Transactions on Instrumentation and Measurement*, vol. 70, pp. 1-7, 2021, Art no. 6007907, doi: 10.1109/TIM.2021.3084292.

[11] K. J. Bois., et al. "Dielectric plug-loaded two-port transmission line measurement technique for dielectric property characterization of granular and liquid materials*." IEEE Transactions on Instrumentation and Measurement* 48.6 (1999): 1141-1148.

[12] J. Baker-Jarvis, M. D. Janezic, J. H. Grosvenor, and R. G. Geyer, *Transmission/reflection and short-circuit line methods for measuring permittivity and permeability*. Boulder, CO: U.S. Dept. of Commerce, Technology Administration, National Institute of Standards and Technology, 1993.

[13] D. M. Pozar, *Microwave Engineering*. Hoboken, New Jersey: Wiley, 2012.

[14] Alkali activated materials: State-of-the-art report, Rilem TC 224-AAM, ed. J.L. Provis and J.S.J. van Deventer. 2014: Springer/RILEM.

[15] Duxson, P., Provis, J.L., Lukey, G.C. and van Deventer, J.S.J., The role of inorganic polymer technology in the development of 'green concrete', Cement and Concrete Research, 2007. 37 (12): pp. 1590-1597.

[16] C. R. Shearer, A. Foudazi, A. Hashemi and K. M. Donnell, "Microwave characterization of fly ash geopolymerization," 2016 IEEE International Instrumentation and Measurement Technology Conference Proceedings, Taipei, Taiwan, 2016, pp. 1-4, doi: 10.1109/I2MTC.2016.7520442.

[17] Donnell, K., Hatfield, S., Zoughi, R. and Kurtis, K., *Wideband microwave characterization of alkali-silica reaction (ASR) gel in cement-based materials,* Materials Letters, 2013. 90: pp. 159-161.

[18] Donnell, K., Zoughi, R. and Kurtis, K., *Demonstration of microwave method for detection of alkali–silica reaction (ASR) gel in cement-based materials,* Cement and Concrete Research, 2013. 44: pp. 1-7.

[19] H. He *et al.*, “Evaluation of five composite dielectric mixing models for understanding relationships between effective permittivity and unfrozen water content,” *Cold Regions Science and Technology*, vol. 130, pp. 33–42, Oct. 2016. doi:10.1016/j.coldregions.2016.07.006

VITA

Jared Daniel Sinkey was born in St. Louis, Missouri. In 2021, he received his BSEE from Missouri University of Science and Technology. Jared worked as an undergraduate in the *u*Sense lab for a short time before continuing his participation in the lab as a graduate student, and pursuing his MSEE at Missouri S&T. He received his Master of Science in Electrical Engineering at Missouri S&T in May 2024.